

A LOW-RANK PROJECTOR-SPLITTING INTEGRATOR FOR THE VLASOV–POISSON EQUATION

LUKAS EINKEMMER*[‡] AND CHRISTIAN LUBICH*

Abstract. Many problems encountered in plasma physics require a description by kinetic equations, which are posed in an up to six-dimensional phase space. A direct discretization of this phase space, often called the Eulerian approach, has many advantages but is extremely expensive from a computational point of view. In the present paper we propose a dynamical low-rank approximation to the Vlasov–Poisson equation, with time integration by a particular splitting method. This approximation is derived by constraining the dynamics to a manifold of low-rank functions via a tangent space projection and by splitting this projection into the subprojections from which it is built. This reduces a time step for the six- (or four-) dimensional Vlasov–Poisson equation to solving two systems of three- (or two-) dimensional advection equations over the time step, once in the position variables and once in the velocity variables, where the size of each system of advection equations is equal to the chosen rank. By a hierarchical dynamical low-rank approximation, a time step for the Vlasov–Poisson equation can be further reduced to a set of six (or four) systems of one-dimensional advection equations, where the size of each system of advection equations is still equal to the rank. The resulting systems of advection equations can then be solved by standard techniques such as semi-Lagrangian or spectral methods. Numerical simulations in two and four dimensions for linear Landau damping, for a two-stream instability and for a plasma echo problem highlight the favorable behavior of this numerical method and show that the proposed algorithm is able to drastically reduce the required computational effort.

Key words. Dynamical low-rank approximation, projector-splitting integrator, Vlasov–Poisson equation.

1. Introduction. Many physical phenomena in both space and laboratory plasmas require a kinetic description. The typical example of such a kinetic model is the Vlasov–Poisson equation

$$\begin{aligned} \partial_t f(t, x, v) + v \cdot \nabla_x f(t, x, v) - E(f)(x) \cdot \nabla_v f(t, x, v) &= 0 \\ \nabla \cdot E(f)(x) &= - \int f(t, x, v) dv + 1, \quad \nabla \times E(f)(x) = 0, \end{aligned} \tag{1.1}$$

which models the time evolution of electrons in a collisionless plasma in the electrostatic regime (assuming a constant background ion density). Equation (1.1) has to be supplemented with appropriate boundary and initial conditions. The particle-density function $f(t, x, v)$, where $x \in \Omega_x \subset \mathbb{R}^d$ and $v \in \Omega_v \subset \mathbb{R}^d$ (with spatial dimension $d \leq 3$), is the quantity to be computed.

In most applications, the primary computational challenge stems from the fact that the equation is posed as an evolution equation in an up to six-dimensional phase space. Thus, direct discretization of the Vlasov–Poisson equation on a grid requires the storage of $\mathcal{O}(n^{2d})$ floating point numbers, where n is the number of grid points per direction. This has been, and in many cases still is, prohibitive from a computational point of view.

Consequently, particle methods are widely used in many application areas that require the numerical solution of kinetic models. Particle methods, such as the particle-in-cell approach, only discretize the physical space x (but not the velocity space v). The v -dependence is approximated by initializing a large number of particles that follow the characteristic curves of equation (1.1). This can significantly reduce the computational cost and has the added benefit that particles congregate in high-density regions of the phase space. However, particle methods suffer from numerical noise that only decreases as the square root in the number of particles. This is, in particular, an issue for problems where the tail of the distribution function has to be resolved accurately. For a detailed discussion the reader is referred to the review article [54].

As an alternative, the entire $2d$ -dimensional phase space can be discretized. This Eulerian approach has received significant attention in recent years. Due to the substantial increase in computational power, four-dimensional simulation can now be performed routinely on high performance computing (HPC) systems. In addition, some five and six-dimensional simulations (usually where in one direction a small number of grid points is sufficient) have been carried out. Nevertheless, these simulations are still extremely costly from a computational point of view. Consequently a significant research effort has been dedicated to improving both

*Mathematisches Institut, Universität Tübingen, Auf der Morgenstelle 10, D-72076 Tübingen, Germany. Email: {einkemmer, lubich}@na.uni-tuebingen.de

[‡]Department of Mathematics, University of Innsbruck, Austria

the numerical algorithms used (see, for example, [9, 15, 13, 19, 23, 30, 46, 49, 50, 53, 3, 7, 52, 5, 6]) as well as the corresponding parallelization to state of the art HPC systems (see, for example, [51, 12, 2, 35, 42, 11, 8]).

The seminal paper [3] introduced a time-splitting approach. This approach has the advantage that the nonlinear Vlasov–Poisson equation can be reduced to a sequence of one-dimensional advection equations (see, for example, [18, 20, 14]). Splitting schemes that have similar properties have been proposed for a range of more complicated models (including the relativistic Vlasov–Maxwell equations [52, 5], drift-kinetic models [23, 7], and gyrokinetic models [22]). This is then usually combined with a semi-Lagrangian discretization of the resulting advection equations. A semi-Lagrangian approach has the advantage that the resulting numerical method is completely free from a Courant–Friedrichs–Lewy (CFL) condition.

Nevertheless, all these methods still incur a computational and storage cost that scales as $\mathcal{O}(n^{2d})$. Thus, it seems natural to ask whether any of the dimension reduction techniques developed for high-dimensional problems are able to help alleviate the computational burden of the Eulerian approach. To understand why it is not entirely clear if such an approach could succeed, we will consider the following equation (with $x, v \in \mathbb{R}$)

$$\partial_t f(t, x, v) + v \partial_x f(t, x, v) = 0.$$

This is just the one-dimensional Vlasov–Poisson equation (1.1) without the nonlinear term. If the initial value $f_0(x, v) = \cos(kx)e^{-v^2/2}$ with $k \in \mathbb{R}$ is imposed, then the exact solution can be easily written down as

$$f(t, x, v) = \cos(k(x - vt))e^{-v^2/2}. \quad (1.2)$$

From this expression we see that, as the system evolves in time, the wave number in the v -direction is given by kt . In particular, we have $\|\partial_v^m f(t, \cdot, \cdot)\| \propto (kt)^m$ which implies that, even though the solution is infinitely often differentiable, smaller and smaller scales appear in phase space. This phenomenon is referred to as filamentation and in many problems a reasonable resolution of these small scale structures is important to obtain physically meaningful results.

A specific problem for sparse-grid approximations is that mixed derivatives (between x and v , but perhaps even more problematic between different v -directions in a multidimensional setting) can be huge. Nevertheless, sparse-grid techniques have been considered for the Vlasov–Poisson equation [34, 10, 24]. A further challenge for these methods is that evaluating the particle-density function (which is required for semi-Lagrangian methods) can be expensive.

Despite these drawbacks, sparse grids can be advantageous in some situations. For example, in [34] first a tensor product decomposition in the x - and v -directions is applied. The remaining d -dimensional problems are then approximated using a sparse grid. For Landau damping in four dimensions this scheme was able to reduce the required memory by approximately a factor of 10 and the run time by a factor of 2. On the other hand, it is somewhat worrying that, as was shown in the cited work, instabilities can develop if not enough degrees of freedom are used. Furthermore, it is well known that sparse grids do not resolve Gaussians very well. This is a problem for kinetic simulations as the steady state is usually a linear combination of Gaussians. In the previously mentioned work, this deficiency is remedied by explicitly incorporating a Gaussian into the numerical method (a so-called δf scheme). However, this approach does not work very well in cases where the particle density significantly deviates from this form.

We now turn to the alternative approach taken in this paper, which appears to be novel for kinetic equations. Computing numerical solutions of high-dimensional evolutionary partial differential equations by *dynamical low-rank approximation* has, however, been investigated extensively in quantum dynamics; see, in particular, [45, 44] for the MCTDH approach to molecular quantum dynamics in the chemical physics literature and [36, 37, 4] for a mathematical point of view to this approach. Some uses of dynamical low-rank approximation in areas outside quantum mechanics are described in [48, 28, 43, 47]. In a general mathematical setting, dynamical low-rank approximation has been studied in [31, 32, 40, 1]. A major algorithmic advance for the time integration was achieved with the projector-splitting methods first proposed in [39] for matrix differential equations and then developed further for various tensor formats in [37, 38, 25, 29, 41]. In the present paper we will adapt such methods to the Vlasov–Poisson equation.

For the Vlasov–Poisson equation, low-rank approximation to the solution is an interesting option for a

number of reasons. First, the solution of our toy problem, given in equation (1.2), can be readily written as

$$f(t, x, v) = (\cos(kx) \cos(kvt) + \sin(kx) \sin(kvt)) e^{-v^2/2}.$$

Thus, the linear part of the equation can be represented exactly with rank two. While this property is lost once we consider the full Vlasov–Poisson equation, it still gives some indication that at least certain types of filamentation can be handled efficiently by the numerical method based on a low-rank approximation. Second, the typical kinetic equilibria formed by linear combination of Gaussians can be very efficiently represented by a low-rank structure. This is in stark contrast to the sparse-grid approach (as has been discussed above).

Recently, in [33] a low-rank numerical algorithm for the Vlasov–Poisson equation has been suggested that first discretizes the problem in time and space. This is done using the common technique of splitting in time and then applying a spline based semi-Lagrangian scheme to the resulting advection equations. Each step of such an algorithm can then be written as a linear combination of low-rank approximations. To avoid that the rank grows during the numerical simulation a singular value decomposition (SVD) is then applied to truncate the low-rank approximation (i.e., approximate it by a different low-rank representation with a fixed rank).

In the present work we consider a different approach to approximating the solution of the Vlasov–Poisson equation by a low-rank representation. We constrain the dynamics of the Vlasov–Poisson equation to a manifold of low-rank functions by a tangent space projection which is then split into its summands over a time step, adapting the projector-splitting approach to time integration of [39]. This yields a sequence of advection equations in a lower-dimensional space. Then an appropriate semi-Lagrangian scheme or even Fourier-based techniques can be applied easily to obtain a numerical solution. This approach is first used to obtain equations separately in x and in v , which reduces a $2d$ -dimensional problem to a sequence of d -dimensional problems (this is the content of Section 2). If r denotes the chosen rank, then over a time step one solves, one after the other,

- a system of r advection equations in x (and computing $2dr^2 + r$ integrals over Ω_v),
- a system of r^2 ordinary differential equations (and computing $2dr^2$ integrals over Ω_x),
- a system of r advection equations in v .

This first-order scheme can be symmetrized to yield a second-order time-stepping scheme. If n degrees of freedom are used in each coordinate direction in the full discretization, then the storage cost is reduced to $O(rn^d)$ from $O(n^{2d})$, and similarly for the number of arithmetic operations.

If appropriate, the procedure can then be repeated in a hierarchical manner in order to reduce the computations further to *one-dimensional* advection equations and *one-dimensional* integrals (this is the content of Section 3). We have chosen a hierarchical Tucker format since the dimensionality at this point in the algorithm is only d and this allows us to treat all coordinate directions in x and in v equally. The algorithm adapts the projector-splitting integrator for low-rank Tucker tensors from [41].

A noteworthy feature of the proposed numerical scheme is that it works entirely within the low-rank manifold. No high-rank tensor needs to be formed and subsequently truncated. This helps to reduce storage and computational cost. In addition, depending on the problem either the physical space or the velocity space or both can be solved directly, while still maintaining the hierarchical low-rank approximation in the other parts of the algorithm.

Numerical simulations for linear Landau damping, a two-stream instability and a plasma echo problem are presented in Section 4. There we show that it is possible to use a small rank to capture the physics of these problems. The proposed numerical method thus substantially reduces the computational cost required to perform the simulation.

2. Description of the numerical algorithm. The goal of this section is to derive an algorithm that approximates the solution of the Vlasov–Poisson equation (1.1) by a low-rank representation. To that end, the approximation to the particle-density function $f(t, x, v)$ is constrained to the following form:

$$f(t, x, v) \approx \sum_{i,j=1}^r X_i(t, x) S_{ij}(t) V_j(t, v), \quad (2.1)$$

where $S_{ij}(t) \in \mathbb{R}$ and we call r the rank of the representation. Note that the dependence of f on the phase space $(x, v) \in \Omega \subset \mathbb{R}^{2d}$ is now approximated by the functions $\{X_i: i = 1, \dots, r\}$ and $\{V_j: j = 1, \dots, r\}$ which depend only on $x \in \Omega_x \subset \mathbb{R}^d$ and $v \in \Omega_v \subset \mathbb{R}^d$, respectively, and on the time t . In the following discussion we always assume that summation indices run from 1 to r and we thus do not specify these bounds.

Now, we seek an approximation to the particle-density function that for all t lies in the set

$$\overline{\mathcal{M}} = \left\{ f \in L^2(\Omega): f(x, v) = \sum_{i,j} X_i(x) S_{ij} V_j(v) \text{ with } S_{ij} \in \mathbb{R}, X_i \in L^2(\Omega_x), V_j \in L^2(\Omega_v) \right\}.$$

It is clear that this representation is not unique. In particular, we can make the assumption that $\langle X_i, X_k \rangle_x = \delta_{ik}$ and $\langle V_j, V_l \rangle_v = \delta_{jl}$, where $\langle \cdot, \cdot \rangle_x$ and $\langle \cdot, \cdot \rangle_v$ are the inner products on $L^2(\Omega_x)$ and $L^2(\Omega_v)$, respectively. We consider a path $f(t)$ on $\overline{\mathcal{M}}$. The corresponding time derivative is denoted by \dot{f} and is of the form

$$\dot{f} = \sum_{i,j} \left(X_i \dot{S}_{ij} V_j + \dot{X}_i S_{ij} V_j + X_i S_{ij} \dot{V}_j \right). \quad (2.2)$$

If we impose the gauge conditions $\langle X_i, \dot{X}_j \rangle_x = 0$ and $\langle V_i, \dot{V}_j \rangle_v = 0$, then \dot{S}_{ij} is uniquely determined by \dot{f} . This follows easily from the fact that

$$\dot{S}_{ij} = \langle X_i V_j, \dot{f} \rangle_{x,v}. \quad (2.3)$$

We then project both sides of equation (2.2) onto X_i and V_j , respectively, and obtain

$$\sum_j S_{ij} \dot{V}_j = \langle X_i, \dot{f} \rangle_x - \sum_j \dot{X}_i S_{ij} V_j, \quad (2.4)$$

$$\sum_i S_{ij} \dot{X}_i = \langle V_j, \dot{f} \rangle_v - \sum_i X_i \dot{S}_{ij}. \quad (2.5)$$

From these relations it follows that the X_i and V_j are uniquely defined if the matrix $S = (S_{ij})$ is invertible. Thus, we seek an approximation that for each time t lies in the manifold

$$\mathcal{M} = \left\{ f \in L^2(\Omega): f(x, v) = \sum_{i,j} X_i(x) S_{ij} V_j(v) \text{ with invertible } S = (S_{ij}) \in \mathbb{R}^{r \times r}, \right. \\ \left. X_i \in L^2(\Omega_x), V_j \in L^2(\Omega_v) \text{ with } \langle X_i, X_k \rangle_x = \delta_{ik}, \langle V_j, V_l \rangle_v = \delta_{jl} \right\}$$

with the corresponding tangent space

$$\mathcal{T}_f \mathcal{M} = \left\{ \dot{f} \in L^2(\Omega): \dot{f}(x, v) = \sum_{i,j} \left(X_i(x) \dot{S}_{ij} V_j(v) + \dot{X}_i(x) S_{ij} V_j(v) + X_i(x) S_{ij} \dot{V}_j(v) \right), \right. \\ \left. \text{with } \dot{S} \in \mathbb{R}^{r \times r}, \dot{X}_i \in L^2(\Omega_x), \dot{V}_j \in L^2(\Omega_v), \text{ and } \langle X_i, \dot{X}_j \rangle_x = 0, \langle V_i, \dot{V}_j \rangle_v = 0 \right\},$$

where f is given by equation (2.1). Now, we consider the reduced dynamics of the Vlasov–Poisson equation on the manifold \mathcal{M} . That is, we consider for the approximate particle density (again denoted by f for ease of notation)

$$\partial_t f = -P(f) (v \cdot \nabla_x f - E(f) \cdot \nabla_v f), \quad (2.6)$$

where $P(f)$ is the orthogonal projector onto the tangent space $\mathcal{T}_f \mathcal{M}$, as defined above.

We will consider the projection $P(f)g$ for a moment. From equations (2.2)–(2.5) we obtain

$$P(f)g = \sum_j \langle V_j, g \rangle_v V_j - \sum_{i,j} X_i \langle X_i V_j, g \rangle_{x,v} V_j + \sum_i X_i \langle X_i, g \rangle_x.$$

Let us introduce the two vector spaces $\bar{X} = \text{span}\{X_i: i = 1, \dots, r\}$ and $\bar{V} = \text{span}\{V_j: j = 1, \dots, r\}$. Then we can write the projector as follows

$$P(f)g = P_{\bar{V}}g - P_{\bar{V}}P_{\bar{X}}g + P_{\bar{X}}g, \quad (2.7)$$

where $P_{\bar{X}}$ is the orthogonal projector onto the vector space \bar{X} , which acts only on the x -variable of $g = g(x, v)$, and $P_{\bar{V}}$ is the orthogonal projector onto the vector space \bar{V} , which acts only on the v -variable of $g(x, v)$. The decomposition of the projector into these three terms forms the basis of our splitting procedure (for matrix differential equations this has been first proposed in [39]).

We proceed by substituting $g = v \cdot \nabla_x f - E(f) \cdot \nabla_v f$ into equation (2.7). This immediately leads to a three-term splitting for equation (2.6). More precisely, for the first-order Lie–Trotter splitting we solve the equations

$$\partial_t f = -P_{\bar{V}}(v \cdot \nabla_x f - E(f) \cdot \nabla_v f), \quad (2.8)$$

$$\partial_t f = P_{\bar{V}}P_{\bar{X}}(v \cdot \nabla_x f - E(f) \cdot \nabla_v f) \quad (2.9)$$

$$\partial_t f = -P_{\bar{X}}(v \cdot \nabla_x f - E(f) \cdot \nabla_v f) \quad (2.10)$$

one after the other. In the following discussion we consider just the first-order Lie–Trotter splitting algorithm with step size τ . The extension to second order (Strang splitting) is nearly straightforward and is presented in Section 2.3.

We assume that the initial value for the algorithm is given in the form

$$f(0, x, v) = \sum_{i,j} X_i^0(x) S_{ij}^0 V_j^0(v).$$

First, let us consider equation (2.8). Since the set $\{V_j: j = 1, \dots, r\}$ forms an orthonormal basis of \bar{V} (for each t), we have for the approximate particle density (again denoted by f)

$$f(t, x, v) = \sum_j K_j(t, x) V_j(t, v), \quad \text{with} \quad K_j(t, x) = \sum_i X_i(t, x) S_{ij}(t), \quad (2.11)$$

where $K_j(t, x)$ is the coefficient of V_j in the corresponding basis expansion. We duly note that K_j is a function of x , but not of v . We then rewrite equation (2.8) as follows

$$\begin{aligned} & \sum_j \partial_t K_j(t, x) V_j(t, v) + \sum_j K_j(t, x) \partial_t V_j(t, v) \\ &= - \sum_j \langle V_j(t, \cdot), v \mapsto v \cdot \nabla_x f(t, x, v) - E(f)(x) \cdot \nabla_v f(t, x, v) \rangle_v V_j(t, v). \end{aligned} \quad (2.12)$$

Note that the electric field is self-consistently determined according to equation (1.1). In practice this is done by solving the Poisson problem $-\Delta\phi = \rho(f) + 1$ for the potential ϕ . The electric field is then determined according to $E = -\nabla\phi$. We discuss how the (electron) charge density $\rho(f) = -\int f(t, x, v) dv$ is computed in terms of the low-rank approximation after stating the corresponding evolution equations (for each step in the splitting algorithm).

The solution of equation (2.12) is given by $V_j(t, v) = V_j(0, v) = V_j^0(v)$ and

$$\partial_t K_j(t, x) = - \sum_l c_{jl}^1 \cdot \nabla_x K_l(t, x) + \sum_l c_{jl}^2 \cdot E(K)(t, x) K_l(t, x) \quad (2.13)$$

with

$$c_{jl}^1 = \int_{\Omega_v} v V_j^0 V_l^0 dv, \quad c_{jl}^2 = \int_{\Omega_v} V_j^0 (\nabla_v V_l^0) dv.$$

The latter is obtained by equating coefficients in the basis expansion. A very useful property of this splitting step is that we have to update only the K_j , but not the V_j . We further note that c_{jl}^1 and c_{jl}^2 are vectors in \mathbb{R}^d , since v and $\nabla_v V_l^0$ are vector quantities. We denote the m th component of c_{jl}^k by $c_{jl}^{k;x_m}$.

In the equation derived above we have written $E(K)$ to denote that the electric field only depends on K during the current step of the algorithm. We will now consider this point in more detail. The electric field is calculated from the electric charge density

$$\rho(f)(t, x) = - \int_{\Omega_v} f(t, x, v) dv$$

as described above. Once the charge ρ is specified, the electric field is uniquely determined. For the purpose of solving equation (2.13) we have the charge

$$\begin{aligned} \rho(t, x) &= - \sum_j K_j(t, x) \int_{\Omega_v} V_j^0(v) dv \\ &= - \sum_j K_j(t, x) \rho(V_j^0). \end{aligned}$$

Thus, the electric field only depends on $K = (K_1, \dots, K_r)$, which explains our notation $E(K)$.

Both solving equation (2.13) and determining the electric field are problems posed in a d -dimensional (as opposed to $2d$ -dimensional) space. Thus, we proceed by integrating equation (2.13) with initial value

$$K_j(0, x) = \sum_i X_i^0(x) S_{ij}^0$$

until time τ to obtain $K_j^1(x) = K_j(\tau, x)$. However, this is not sufficient as the K_j^1 are not necessarily orthogonal (a requirement of our low-rank representation). Fortunately, this is easily remedied by performing a QR decomposition

$$K_j^1(x) = \sum_i X_i^1(x) \hat{S}_{ij}^1$$

to obtain orthonormal X_i^1 and the matrix \hat{S}_{ij}^1 . Once a space discretization has been introduced, this QR decomposition can be simply computed by using an appropriate function from a software package such as LAPACK. However, from a mathematical point of view, the continuous dependence on x causes no issues. For example, the modified Gram-Schmidt process works just as well in the continuous formulation considered here.

Second, we proceed in a similar way for equation (2.9). In this case both V_j^0 and X_i^1 are unchanged and only S_{ij} is updated. The corresponding evolution equation (which runs backward in time) is given by

$$\begin{aligned} \partial_t S_{ij}(t) &= \langle X_i^1(x) V_j^0(v), (v \cdot \nabla_x - E(S)(t, x) \cdot \nabla_v) \sum_{k,l} X_k^1(x) S_{kl}(t) V_l^0(v) \rangle_{x,v} \\ &= \sum_{k,l} (c_{jl}^1 \cdot d_{ik}^2 - c_{jl}^2 \cdot d_{ik}^1 [E(S(t))]) S_{kl}(t) \end{aligned} \quad (2.14)$$

with

$$d_{ik}^1[E] = \int_{\Omega_x} X_i^1 E X_k^1 dx, \quad d_{ik}^2 = \int_{\Omega_x} X_i^1 (\nabla_x X_k^1) dx,$$

and $E(S(t))$ denotes the electric field corresponding to the charge density

$$\rho(t, x) = - \sum_{i,j} X_i^1(x) S_{ij}(t) \rho(V_j^0).$$

Note that in this case the evolution equation depends neither on x nor on v . Since E and $\nabla_x X_k^1$ are vector quantities, we have coefficient vectors d_{ik}^1 and d_{ik}^2 in \mathbb{R}^d . We now integrate equation (2.14) with initial value $S_{ij}(0) = \widehat{S}_{ij}^1$ until time τ obtain $\widetilde{S}_{ij}^0 = S_{ij}(\tau)$. This completes the second step of the algorithm.

Finally, we consider equation (2.10). Similar to the first step we have

$$f(t, x, v) \approx \sum_i X_i(t, x) L_i(t, v), \quad \text{with} \quad L_i(t, v) = \sum_j S_{ij}(t) V_j(t, v).$$

As before, it is easy to show that this time the X_i remain constant during that step. Thus, the L_j satisfy the following evolution equation

$$\begin{aligned} \partial_t L_i(t, v) &= - \left\langle X_j^1, (v \cdot \nabla_x - E(L)(x, t) \cdot \nabla_v) \sum_k X_k^1 L_k(t, v) \right\rangle_x \\ &= \sum_k d_{ik}^1 [E(L(t, \cdot))] \cdot \nabla_v L_k(t, v) - \sum_k (d_{ik}^2 \cdot v) L_k(t, v), \end{aligned} \quad (2.15)$$

where $E(L(t, \cdot))$ denotes the electric field that corresponds to the charge density

$$\rho(t, x) = - \sum_i X_i^1(x) \rho(L_i(t, \cdot)).$$

We then integrate equation (2.15) with initial value

$$L_i(0, v) = \sum_j \widetilde{S}_{ij}^0 V_j^0(v)$$

up to time τ to obtain $L_i^1(v) = L_i(\tau, v)$. Since, in general, the L_i^1 are not orthogonal we have to perform a QR decomposition

$$L_i^1(v) = \sum_j S_{ij}^1 V_j^1(v)$$

to obtain orthonormal functions V_j^1 and the matrix S_{ij}^1 . Finally, the output of our Lie splitting algorithm is

$$f(\tau, x, v) \approx \sum_{i,j} X_i^1(x) S_{ij}^1 V_j^1(v).$$

To render this algorithm into a numerical scheme that can be implemented on a computer, we have to discretize in space. In principle, it is then possible to integrate equations (2.13), (2.14), and (2.15) using an arbitrary time stepping method. However, equations (2.13) and (2.15) share many common features with the original Vlasov system. Therefore, employing a numerical method tailored to the present situation can result in significant performance improvements. More precisely, we will consider fast Fourier based techniques (Section 2.1) and a semi-Lagrangian approach (Section 2.2). Both of these schemes remove the CFL condition from equations (2.13) and (2.15). Similar methods have been extensively used for direct Eulerian simulation of the Vlasov equation (which is the primary motivation to extend them to the low-rank algorithm proposed in this work).

Before proceeding, however, let us briefly discuss the complexity of our algorithm. For that purpose we choose to discretize both x and v using n grid points in every coordinate direction. The storage cost of our numerical method is then $\mathcal{O}(n^d r)$, compared to $\mathcal{O}(n^{2d})$ for the Eulerian approach. Now, let us assume that the cost of solving the evolution equations is proportional to the degrees of freedom (which is usually true for semi-Lagrangian schemes and true up to a logarithm for spectral methods). In this case our low-rank algorithm requires $\mathcal{O}(n^d r)$ arithmetic operations for the evolution equations and $\mathcal{O}(n^d r^2)$ operations for computing the integrals, compared to $\mathcal{O}(n^{2d})$ for a direct simulation.

2.1. Spectral method. In the framework of the classic splitting algorithm for the Vlasov–Poisson equation (which goes back to [3]), spectral methods have long been considered a viable approach. This is mainly due to the fact that once the splitting has been performed, the remaining advection equations can be solved efficiently by employing fast Fourier transforms. Equations (2.13) and (2.15) are somewhat more complicated, compared to the advection equations resulting from a direct splitting of the Vlasov–Poisson equation, in that a nonlinear term is added. In addition, for equation (2.15) even the speed of the advection depends on the electric field. However, since the advection coefficients are scalar quantities it is still possible to apply Fourier techniques, as we will show below.

We first consider equation (2.13). Performing a Fourier transform (denoted by \mathcal{F}) in x yields

$$\partial_t \hat{K}_j(t, k) = - \sum_{\beta} (c_{j\beta}^1 \cdot ik) \hat{K}_\beta(t, k) + \sum_l c_{jl}^2 \cdot \mathcal{F}(E(K)(\cdot) K_l(t, \cdot)).$$

Forming the vectors $\hat{K} = (\hat{K}_1, \dots, \hat{K}_r)$ and $K = (K_1, \dots, K_r)$ and defining F appropriately, we can write this in matrix notation

$$\dot{\hat{K}}(t, k) = A(k) \hat{K}(t, k) + F(\hat{K}(t, \cdot))(k). \quad (2.16)$$

The linear part is the only source of stiffness. For each k we have $A(k) \in \mathbb{R}^{r \times r}$ which is a small enough matrix to be handled by direct methods. Thus, an exponential integrator is easily able to integrate the linear part exactly (which removes the CFL condition). For a first order scheme the exponential Euler method is sufficient

$$\hat{K}(\tau, k) \approx e^{\tau A(k)} \hat{K}(0, k) + \tau \varphi_1(\tau A(k)) F(\hat{K}(0, \cdot))(k),$$

where $\varphi_1(z) = (e^z - 1)/z$ is an entire function. It should be noted that higher order methods have been derived as well (see, for example, the review article [26]).

Now, let us turn our attention to equation (2.15). Before this equation can be made amenable to Fourier techniques, a further approximation has to be performed. Specifically, we freeze the electric field at the beginning of the time step. That is, instead of equation (2.15) we solve the approximation

$$\partial_t L_i(t, v) = \sum_k d_{ik}^1 \cdot \nabla_v L_k(t, v) - \sum_k (d_{ik}^2 \cdot v) L_k(t, v)$$

with $d_{ik}^1 = d_{ik}^1(E(L(0, \cdot)))$. This still yields a first order approximation. We will show in Section 2.3 how this technique can be improved to second order. Now, the advection speed is independent of L and we are able to apply a Fourier transform in v which yields

$$\partial_t \hat{L}_i(t, k) = \sum_k (d_{ik}^1 \cdot ik) \hat{L}_k(t, k) - \sum_k d_{ik}^2 \cdot \mathcal{F}(v L_k(t, \cdot)).$$

This is in the form of equation (2.16) and can thus be handled by an exponential integrator in the same way as is explained above.

2.2. Semi-Lagrangian method. Semi-Lagrangian methods are widely employed to solve the Vlasov equation. To a large part this is due to the fact that by performing a splitting in the different spatial and velocity directions, only one-dimensional advection equations have to be solved. The projection operation necessary for these class of methods can then be implemented easily and efficiently. In the present section our goal is to show that an efficient semi-Lagrangian scheme can be derived for equations (2.13) and (2.15).

We start with equation (2.13) and use the vector notation $K = (K_1, \dots, K_r)$. Then,

$$\partial_t K(t, x) = -c^{1;x_1} \partial_{x_1} K(t, x) - c^{1;x_2} \partial_{x_2} K(t, x) - c^{1;x_3} \partial_{x_3} K(t, x) + (c^2 \cdot E(K)(t, x)) K(t, x). \quad (2.17)$$

Applying a first order Lie splitting to equation (2.17), with initial value $K(0, x) = K^0(x)$, gives

$$K(\tau, \cdot) \approx e^{-\tau c^{1;x_1} \partial_{x_1}} e^{-\tau c^{1;x_2} \partial_{x_2}} e^{-\tau c^{1;x_3} \partial_{x_3}} (K^0 + \tau (c^2 \cdot E(K^0)) K^0).$$

This can be extended trivially to second or higher order. The crucial part is the computation of

$$M(t, x) = e^{-tc^{1;x_1}\partial_{x_1}} M(0, x)$$

which is equivalent to the partial differential equation

$$\partial_t M(t, x) = -c^{1;x_1}\partial_{x_1} M(t, x).$$

Since $c^{1;x_1}$ is symmetric, there exists an orthogonal matrix T such that $Tc^{1;x_1}T^T = D$, where D is a diagonal matrix. All these computations can be done efficiently as $c^{1;x_1} \in \mathbb{R}^{r \times r}$ (i.e. we are dealing with small matrices). We now change variables to $\bar{M} = TM$ and obtain

$$\partial_t \bar{M}_j(t, x) = -D_{jj}\partial_{x_1} \bar{M}(t, x).$$

This is a one-dimensional advection equation with constants coefficients and can thus be treated with an arbitrary semi-Lagrangian method. Once $\bar{M}(\tau, x)$ is obtained the coordinate transformation is undone such that we get $M_j(\tau, x) = T^T \bar{M}_j(\tau, x)$. Exactly the same procedure is then applied to the advection in the x_2 and x_3 direction.

For equation (2.15) we proceed in a similar way. The main difference here is that we first freeze $d_{ik}^1 = d_{ik}^1(E(L(0, \cdot)))$ at the beginning of the step (as is explained in more detail in the previous section). This leaves us with

$$\partial_t L_i(t, v) = \sum_k d_{ik}^1 \cdot \nabla_v L_k(t, v) - \sum_k (d_{ik}^2 \cdot v) L_k(t, v).$$

Since this equation is (almost) identical to equation (2.17) and $d^{1;x_1}$, $d^{1;x_2}$, and $d^{1;x_3}$ are symmetric, we can apply the same algorithm.

2.3. Second-order integrator. So far we have only considered the first order Lie splitting. However, in principle it is simple to employ the second order Strang splitting. The main obstacle in this case is that for both the Fourier approach (introduced in section 2.1) and the semi-Lagrangian approach (introduced in section 2.2) it is essential that a further approximation is made when solving equation (2.15). More specifically, the electric field E is assumed fixed during that step. Thus, a naive application of Strang splitting would still only result in a first order method. However, in [17, 16] a technique has been developed that can overcome this difficulty for methods of arbitrary order.

A detailed account of the second order accurate scheme is given in Algorithm 1. From there it should also be clear that no additional ingredients, compared to the first order scheme described in section 2, are needed. The main point is that we use an embedded Lie scheme of step size $\tau/2$ in order to determine an electric field $E^{1/2}$ such that $E^{1/2}(x) \approx E(f(\frac{\tau}{2}, \cdot))(x)$. Using $E^{1/2}$ in the middle step of the Strang splitting, which approximates equation (2.15), yields a numerical method that is almost symmetric. Then composing two Lie steps in opposite order yields a second order method.

3. A hierarchical low-rank algorithm. The algorithm proposed in the previous section reduces a $2d$ -dimensional problem to a number of d -dimensional problems. However, if the solution under consideration also admits a low-rank structure in $X_i(t, x)$ and $V_j(t, v)$, it is possible to further reduce the dimensionality of the equations that need to be solved. To derive such an algorithm is the content of the present section. We will first consider the four-dimensional case ($d = 2$). This is sufficient to elucidate the important aspects of the algorithm. The algorithm for the six-dimensional ($d = 3$) case is stated in Section 3.2.

3.1. The hierarchical low-rank algorithm in four dimensions. Once again we start from the low-rank approximation

$$f(t, x, v) \approx \sum_{i,j} X_i(t, x) S_{ij}(t) V_j(t, v), \quad (3.1)$$

where $x = (x_1, x_2) \in \Omega_x \subset \mathbb{R}^2$, $v = (v_1, v_2) \in \Omega_v \subset \mathbb{R}^2$, and $S \in \mathbb{R}^{r \times r}$. In addition, we will now restrict X_i and V_j to the low-rank representations

$$X_i(t, x) = \sum_{\alpha, \beta} X_{1\alpha}(t, x_1) C_{i\alpha\beta}(t) X_{2\beta}(t, x_2) \quad (3.2)$$

Algorithm 1 A second-order accurate low-rank algorithm for the Vlasov–Poisson equation.

Input: X_i^0, S_{ij}^0, V_j^0 (such that $f(0, x, v) \approx \sum_{i,j} X_i^0(x) S_{ij}^0 V_j^0(v)$)

Output: X_i^2, S_{ij}^5, V_j^1 (such that $f(\tau, x, v) \approx \sum_{i,j} X_i^2(x) S_{ij}^5 V_j^1(v)$)

- 1: Solve equation (2.13) with initial value $\sum_i X_i^0 S_{ij}^0$ up to time $\tau/2$ to obtain K_j^1 .
 - 2: Perform a QR decomposition of K_j^1 to obtain X_i^1 and S_{ij}^1 .
 - 3: Solve equation (2.14) with initial value S_{ij}^1 up to time $\tau/2$ to obtain S_{ij}^2 .
 - 4: Compute the electric field E using X_i^1, S_{ij}^2 , and V_j^0 .
 - 5: Compute d_{ij}^1 using E .
 - 6: Solve equation (2.15) with fixed d_{ij}^1 and initial value $\sum_j S_{ij}^2 V_j^0$ up to time $\tau/2$ to obtain $L_i^{1/2}$.
 - 7: Compute the electric field $E^{1/2}$ using $L_i^{1/2}$ and X_i^1 .
 - 8: Compute d_{ij}^1 using $E^{1/2}$.
 - 9: Solve equation (2.15) with the fixed d_{ij}^1 and initial value $\sum_j S_{ij}^2 V_j^0$ up to time τ to obtain L_i^1 .
 - 10: Perform a QR decomposition of L_i^1 to obtain V_j^1 and S_{ij}^3 .
 - 11: Solve equation (2.14) with initial value S_{ij}^3 up to time $\tau/2$ to obtain S_{ij}^4 .
 - 12: Solve equation (2.13) with initial value $\sum_i X_i^1 S_{ij}^4$ up to time $\tau/2$ to obtain K_j^2 .
 - 13: Perform a QR decomposition of K_j^2 to obtain X_i^2 and S_{ij}^5 .
-

and

$$V_j(t, v) = \sum_{\alpha, \beta} V_{1\alpha}(t, v_1) D_{j\alpha\beta}(t) V_{2\beta}(t, v_2), \quad (3.3)$$

where $C \in \mathbb{R}^{r \times r_x \times r_x}$, $D \in \mathbb{R}^{r \times r_v \times r_v}$ and r_x and r_v is the rank in the x - and v -direction, respectively. It is, however, entirely reasonable for the Vlasov equation that, for example, a further low-rank structure is present in velocity space but the same is not true in physical space. As an example, consider a plasma system, where only weak kinetic effects are present. Traditionally, fluid models (such as magnetohydrodynamics and its extensions) have been used to model such systems. However, this approach neglects kinetic effects altogether. As an alternative the low-rank approach in this paper could be employed. Since the system is still close to thermodynamic equilibrium, a further low-rank approximation can be employed in v . On the other hand, the dynamics in x might not be accessible to such an approximation. In this case only the hierarchical low-rank representation given in (3.3) would be used. This would leave equation (2.13) precisely as stated in Section 2, while equation (2.15) is replaced by the algorithm developed in this section.

Fortunately, equations (2.13) and (2.15) are sufficiently similar that we only have to derive (and perhaps more importantly, implement) the algorithm once. Thus, we will consider the following equation

$$\partial_t K_j(t, x) = - \sum_l c_{jl}^1 \cdot \nabla_x K_l(t, x) - \sum_l c_{jl}^2 \cdot F(K)(x) K_l(t, x).$$

For solving equation (2.13) we simply set $F(K) = -E(K)$. If we replace c^1 and c^2 by d^1 and d^2 , respectively, replace the variable x by v , reverse the sign of the equation, and set $F(K)(v) = v$, then we obtain precisely equation (2.15).

In the following we transfer the algorithm proposed for time integration of Tucker tensors in [41] to the current setting. The reader is encouraged to first look up [41] before entering into the thicket of formulas presented in the following. Compared to the generic case in [41], there are important simplifications for the problem under consideration, which even influence the representation of our low-rank approximation. In fact, a Tucker representation for the order-three tensor $X_j(t, x_1, x_2)$ (for fixed t) would be given by

$$X_j(t, x) = \sum_{l, \alpha, \beta} R_{l\alpha\beta}(t) A_{lj}(t) X_{1\alpha}(t, x_1) X_{2\beta}(t, x_2)$$

and not by equation (3.2). The algorithm would then proceed by updating A , X_1 , X_2 , and finally the core tensor R . However, in the present setting A is artificial in the sense that we can always go back to the

representation in equation (3.2) by setting

$$C_{j\alpha\beta}(t) = \sum_l R_{l\alpha\beta}(t) A_{lj}(t).$$

If we want to express this in the Tucker format, we can insert an identity matrix

$$X_j(t, x) = \sum_{l, \alpha, \beta} C_{l\alpha\beta}(t) \delta_{lj} X_\alpha^1(x_1) X_\beta^2(x_2).$$

It is straightforward to show that if we apply the projection splitting algorithm in [41] to a Tucker tensor in this form, the first step leaves both C and A (in this case the identity) unchanged. Thus, we can proceed with the algorithm and work directly in the representation given by (3.2). In the following we will consider the first-order Lie–Trotter splitting. We assume that the initial value is given in the form

$$f(0, x, v) = \sum_{i,j} X_i^0(x) S_{ij}^0 V_j^0(v) \quad (3.4)$$

with

$$X_i^0(x) = \sum_{\alpha, \beta} X_{1\alpha}^0(x_1) G_{i\alpha\beta}^0 X_{2\beta}^0(x_2). \quad (3.5)$$

Since the evolution equation is formulated for $K_j = \sum_i X_i S_{ij}$, we then compute

$$K_j^0(x) = \sum_{\alpha, \beta} X_{1\alpha}^0(x_1) C_{j\alpha\beta}^0 X_{2\beta}^0(x_2),$$

where

$$C_{j\alpha\beta}^0 = \sum_i G_{i\alpha\beta}^0 S_{ij}^0.$$

Step 1: The first step of the algorithm updates X_1 and C . First, we perform a QR decomposition

$$C_{j\alpha\beta}^0 = \sum_\xi Q_{j\xi\beta} R_{\alpha\xi}^0$$

and set

$$W_{j\xi}(x_2) = \sum_\beta Q_{j\xi\beta} X_{2\beta}^0(x_2). \quad (3.6)$$

In an actual implementation, the QR decomposition can be computed by defining $A \in \mathbb{R}^{(r \cdot r_x) \times r_x}$ such that $A_{(j+\beta r)\alpha} = C_{j\alpha\beta}^0$ and then computing the QR decomposition of A . Now, let us define

$$M_\alpha(t, x_1) = \sum_\xi X_{1\xi}(t, x_1) R_{\xi\alpha}(t),$$

for which we give an evolution equation. These M_α in fact play the same role as the K_j did in the algorithm of Section 2. The equation derived is as follows:

$$\begin{aligned} \partial_t M_\alpha(t, x_1) &= - \sum_i \left\langle W_{i\alpha}, \sum_k (c_{ik}^1 \cdot \nabla_x + c_{ik}^2 \cdot F(M)(x_1, \cdot)) \sum_\xi M_\xi(t, x_1) W_{k\xi} \right\rangle_{x_2} \\ &= - \sum_\xi a_{\alpha\xi}^1 \partial_{x_1} M_\xi(t, x_1) - \sum_\xi (a_{\alpha\xi}^2 + a_{\alpha\xi}^3(x_1)) M_\xi(t, x_1), \end{aligned} \quad (3.7)$$

where

$$a_{\alpha\xi}^1 = \sum_{i,k} c_{ik}^{1;x_1} \langle W_{i\alpha}, W_{k\xi} \rangle_{x_2}, \quad a_{\alpha\xi}^2 = \sum_{i,k} c_{ik}^{1;x_2} \langle W_{i\alpha}, \partial_{x_2} W_{k\xi} \rangle_{x_2},$$

and

$$a_{\alpha\xi}^3(x_1) = \sum_{i,k} c_{ik}^2 \cdot \langle W_{i\alpha}, F(M)(x_1, \cdot) W_{k\xi} \rangle_{x_2}.$$

Note that a^1 , a^2 , and a^3 can be easily expressed in terms of Q and inner products over functions involving $X_{2\beta}$. For $a_{\alpha\beta}^1$ the orthonormality relation of the $X_{2\beta}$ can be used to obtain a simpler formula that can be computed without performing any integrals:

$$a_{\alpha\xi}^1 = \sum_{i,k,\beta} c_{ik}^{1;x} Q_{i\alpha\beta} Q_{k\xi\beta}.$$

For a^2 we have

$$a_{\alpha\xi}^2 = \sum_{k,\beta} \left(\sum_i c_{ik}^{1;x_2} Q_{i\alpha\beta} \right) \left(\sum_{\eta} Q_{k\xi\eta} \langle X_{2\beta}^0, \partial_{x_2} X_{2\eta}^0 \rangle_{x_2} \right)$$

which requires $\mathcal{O}(n\mathcal{R}^2)$, with $\mathcal{R} = \max(r, r_x, r_v)$, arithmetic operations to compute the integrals and then $\mathcal{O}(\mathcal{R}^4)$ operations to obtain the entries $a_{\alpha\xi}^2$. A similar formula can be given for a^3 but we postpone this discussion until later (where we will also discuss the low-rank representation of the electric field in more detail).

Now, we solve equation (3.7) with initial value

$$M_\alpha(0, x_1) = \sum_{\xi} X_{1\xi}^0(x_1) R_{\xi\alpha}^0$$

until time τ and obtain $M_\alpha^1(x_1) = M_\alpha(\tau, x_1)$. Then a QR factorization

$$M_\alpha^1(x_1) = \sum_{\xi} X_{1\xi}^1(x_1) R_{\xi\alpha}^1$$

is performed to obtain orthonormal functions $X_{1\xi}^1$ and the matrix R^1 .

Now, an evolution equation for R is derived to become

$$\begin{aligned} \dot{R}_{\xi\alpha}(t) &= \sum_i \left\langle X_{1\xi}^1 W_{i\alpha}, \sum_k (c_{ik}^1 \cdot \nabla_x + c_{ik}^2 \cdot F(R)) \sum_{\xi', \alpha'} X_{1\xi'}^1 R_{\xi'\alpha'}(t) W_{k\alpha'} \right\rangle_x \\ &= \sum_{\xi', \alpha'} b_{\xi\xi'}^1 R_{\xi'\alpha'}(t) a_{\alpha\alpha'}^1 + \sum_{\alpha'} R_{\xi\alpha'}(t) a_{\alpha\alpha'}^2 + \sum_{\xi', \alpha'} B_{\xi\alpha\xi'\alpha'} R_{\xi'\alpha'}(t) \end{aligned} \quad (3.8)$$

with

$$b_{\xi\xi'}^1 = \langle X_{1\xi}^1, \partial_{x_1} X_{1\xi'}^1 \rangle_{x_1}, \quad B_{\xi\alpha\xi'\alpha'} = \sum_{i,k} c_{ik}^2 \cdot \langle X_{1\xi}^1 W_{i\alpha}, F(R) X_{1\xi'}^1 W_{k\alpha'} \rangle_x.$$

Let us note that $B_{\xi\alpha\xi'\alpha'}$ is defined by a two-dimensional integral. However, it is, of course, possible to also obtain a low-rank approximation for $F(R)$. Only two cases are relevant here. First, $F(x) = x$ which trivially is a low-rank approximation of rank 1. Second, $F(R) = -E(R)$. Then, the electric field E is approximated by

$$E(x_1, x_2) = \sum_{\mu} E_{1\mu}(x_1) \circ E_{2\mu}(x_2),$$

where the component-wise product is written as \circ and $\mu = 1, \dots, r_E$; here r_E is the rank used to represent the electric field. Then

$$B_{\xi\alpha\xi'\alpha'} = - \sum_{i,k,\mu} c_{ik}^2 \langle X_{1\xi}^1, E_{1\mu} X_{1\xi'}^1 \rangle_{x_1} \circ \langle W_{i\alpha}, E_{2\mu} W_{k\alpha'} \rangle_{x_2}, \quad (3.9)$$

which only requires the evaluation of one-dimensional integrals. Nevertheless, evaluating equation (3.9) naively requires $\mathcal{O}(\mathcal{R}^7)$ arithmetic operations (with $\mathcal{R} = \max(r, r_x, r_E)$), in addition to evaluating the integrals. However, we can write

$$B_{\xi\alpha\xi'\alpha'} = - \sum_{\mu} \langle X_{1\xi}^1, E_{1\mu} X_{1\xi'}^1 \rangle_{x_1} \cdot \sum_{i,k} c_{ik}^2 \langle W_{i\alpha}, E_{2\mu} W_{k\alpha'} \rangle_{x_2}$$

and evaluate the sums from right to left, which only requires $\mathcal{O}(\mathcal{R}^5)$ arithmetic operations.

Now, we integrate equation (3.8) with initial value $R_{\xi\alpha}(0) = R_{\xi\alpha}^1$ until time τ to obtain $R_{\xi\alpha}^2 = R_{\xi\alpha}(\tau)$. From this we update C as

$$C_{j\alpha\beta}^1 = \sum_{\xi} Q_{j\xi\beta} R_{\alpha\xi}^2,$$

which completes the first step of the algorithm.

Step 2: The second step proceeds in a similar manner, but updates X_2 and C . First, we perform a QR decomposition

$$C_{i\alpha\beta}^1 = \sum_{\eta} Q_{i\alpha\eta} R_{\beta\eta}^0.$$

The tensor Q and the matrix R^0 obtained here are different from those in the first step, but for ease of notation we do not use different symbols or extra superscripts. We define

$$N_{\beta}(t, x_2) = \sum_{\eta} X_{2\eta}(t, x_2) R_{\eta\beta}(t)$$

for which we determine an evolution equation. These N_{β} play the same role as the L_j did in the algorithm of Section 2. The equation derived is as follows:

$$\begin{aligned} \partial_t N_{\beta}(t, x_2) &= - \sum_{i,\alpha} Q_{i\alpha\beta} \left\langle X_{1\alpha}^1, \sum_k (c_{ik}^1 \cdot \nabla_x + c_{ik}^2 \cdot F(N)) \sum_{\xi,\eta} X_{1\xi}^1 Q_{k\xi\eta} N_{\eta}(t, x_2) \right\rangle_{x_1} \\ &= - \sum_{\eta} h_{\beta\eta}^1 \partial_{x_2} N_{\eta}(t, x_2) - \sum_{\eta} (h_{\beta\eta}^2 + h_{\beta\eta}^3(x_2)) N_{\eta}(t, x_2), \end{aligned} \quad (3.10)$$

where

$$h_{\beta\eta}^1 = \sum_{i,k,\alpha} c_{ik}^{1;x_2} Q_{i\alpha\beta} Q_{k\alpha\eta}, \quad h_{\beta\eta}^2 = \sum_{i,k,\alpha,\xi} Q_{i\alpha\beta} Q_{k\xi\eta} c_{ik}^{1;x_1} b_{\alpha\xi}^1$$

and

$$h_{\beta\eta}^3(x_2) = \sum_{i,k,\alpha,\xi} Q_{i\alpha\beta} Q_{k\xi\eta} c_{ik}^2 \cdot \langle X_{1\alpha}^1, F(N)(\cdot, x_2) X_{1\xi}^1 \rangle_{x_1}.$$

Equation (3.10) is integrated with initial value

$$N_{\beta}(0, x_2) = \sum_{\eta} X_{2\eta}^0(x_2) R_{\eta\beta}^0$$

until time τ . We then set $N_\beta^1(x_2) = N_\beta(\tau, x_2)$ and perform a QR decomposition

$$N_\beta^1 = \sum_{\eta} X_{2\eta}^1 R_{\eta\beta}^1$$

to obtain orthonormal functions $X_{2\eta}^1$ and the matrix R^1 . Next, an evolution equation for R is obtained as follows:

$$\begin{aligned} \dot{R}_{\eta\beta}(t) &= \sum_{i,\alpha} Q_{i\alpha\beta} \left\langle X_{1\alpha}^1 X_{2\eta}^1, \sum_k (c_{ik}^1 \cdot \nabla_x + c_{ik}^2 \cdot F(R)) \sum_{\alpha', \eta', \beta'} X_{1\alpha'}^1 Q_{k\alpha'\beta'} R_{\eta'\beta'} X_{2\eta'}^1 \right\rangle_{x_1, x_2} \\ &= \sum_{\eta', \beta'} d_{\eta\eta'}^1 R_{\eta'\beta'}(t) h_{\beta\beta'}^1 + \sum_{\beta'} R_{\eta\beta'}(t) h_{\beta\beta'}^2 + \sum_{\eta', \beta'} G_{\eta\beta\eta'\beta'} R_{\eta'\beta'}(t) \end{aligned} \quad (3.11)$$

with

$$d_{\eta\eta'}^1 = \langle X_{2\eta}^1, \partial_{x_2} X_{2\eta'}^1 \rangle_{x_2}, \quad G_{\eta\beta\eta'\beta'} = \sum_{i,k,\alpha,\alpha'} Q_{i\alpha\beta} Q_{k\alpha'\beta'} c_{ik}^2 \cdot \langle X_{1\alpha}^1 X_{2\eta}^1, F(R) X_{1\alpha'}^1 X_{2\eta'}^1 \rangle_{x_1, x_2}.$$

We then integrate equation (3.11) with initial value R^1 up to time τ and set $R_{\eta\beta}^2 = R_{\eta\beta}(\tau)$. We then update the core tensor C as

$$C_{i\alpha\beta}^2 = \sum_{\eta} Q_{i\alpha\eta} R_{\beta\eta}^2.$$

This completes the second step of the algorithm.

Step 3: In the last step we update C and the matrix S . The tensor C is first updated by the following evolution equation:

$$\begin{aligned} \dot{C}_{i\alpha\beta}(t) &= - \left\langle X_{1\alpha}^1 X_{2\beta}^1, \sum_k (c_{ik}^1 \cdot \nabla_x + c_{ik}^2 \cdot F(C)) \sum_{\xi, \eta} X_{1\xi}^1 C_{k\xi\eta}(t) X_{2\eta}^1 \right\rangle_x \\ &= - \sum_{k, \xi} c_{ik}^{1;x_1} b_{\alpha\xi}^1 C_{k\xi\beta}(t) - \sum_{k, \eta} c_{ik}^{1;x_2} d_{\beta\eta}^1 C_{k\alpha\eta}(t) - \sum_{k, \xi, \eta} (c_{ik}^2 \cdot e_{\alpha\beta\xi\eta}) C_{k\xi\eta}(t), \end{aligned} \quad (3.12)$$

where

$$e_{\alpha\beta\xi\eta} = \langle X_{1\alpha} X_{2\beta}, F(C) X_{1\xi} X_{2\eta} \rangle_x.$$

We integrate equation (3.12) with initial value C^2 until time τ and set $C_{i\alpha\beta}^3 = C_{i\alpha\beta}(\tau)$. Now, we have obtained the following representation

$$K_j(\tau, x) \approx K_j^1(x) = \sum_{\alpha, \beta} X_{1\alpha}^1(x_1) C_{j\alpha\beta}^3 X_{2\beta}^1(x_2).$$

This, however, is not yet sufficient, since in order to obtain an approximation in the form given by equation (3.1), we have to perform a QR decomposition. If this is done naively, the complexity would scale as n^d , with n the number of grid points per direction, which is precisely what we want to avoid in the present setting. However, since the X_1^1 and X_2^1 are already orthogonalized, we can compute a QR decomposition without modifying X_1^1 or X_2^1 and without evaluating any integrals. This is accomplished, for example, by carrying out the modified Gram-Schmidt process. To perform the Gram-Schmidt process, inner products and linear combinations of the different K_j^1 are required. However, since by orthogonality

$$\begin{aligned} \langle K_j^1, K_k^1 \rangle_x &= \sum_{\alpha\beta\xi\eta} C_{j\alpha\beta}^3 C_{k\xi\eta}^3 \langle X_{1\alpha}^1, X_{1\xi}^1 \rangle_{x_1} \langle X_{2\beta}^1, X_{2\eta}^1 \rangle_{x_2} \\ &= \sum_{\alpha, \beta} C_{j\alpha\beta}^3 C_{k\alpha\beta}^3 \end{aligned} \quad (3.13)$$

and since

$$K_j^1 + cK_k^1 = \sum_{\alpha,\beta} X_{1\alpha}^1(x_1) C_{\alpha\beta}^+ X_{2\beta}^1(x_2) \quad \text{with} \quad C_{\alpha\beta}^+ = C_{j\alpha\beta}^3 + cC_{k\alpha\beta}^3, \quad (3.14)$$

this can be done efficiently, as only operations on C have to be performed. The corresponding procedure is shown in Algorithm 2 and requires \mathcal{R}^4 arithmetic operations. It is applied to the input $C_{j\alpha\beta}^3$ and results in the output $C_{j\alpha\beta}^4$ and S_{ij}^1 (in an actual implementation this can be done in place, as is demonstrated by 2). Thus, we finally obtain the low-rank representation

$$f(0, x, v) = \sum_{i,j} X_i^1(x) S_{ij}^1 V_j^1(v)$$

with

$$X_i^1(x) = \sum_{\alpha,\beta} X_{1\alpha}^1(x_1) C_{i\alpha\beta}^4 X_{2\beta}^1(x_2).$$

This is precisely the same form in which the initial value is provided, see equations (3.4) and (3.5). We then can proceed to apply the corresponding procedure to update the quantities depending on velocity space.

Algorithm 2 The goal of the algorithm is to obtain X_i and S_{ij} such that $\langle X_i, X_k \rangle_x = \delta_{ik}$ and $K_j = \sum_i X_i S_{ij}$ with $X_i = \sum_{\alpha,\beta} X_{1\alpha}^1 C_{i\alpha\beta} X_{2\beta}^1$. The input is such that $K_j = \sum_{\alpha,\beta} X_{1\alpha}^1 C_{j\alpha\beta} X_{2\beta}^1$ and consequently only C is modified by the algorithm. This is accomplished using the modified Gram-Schmidt procedure and equations (3.13) and (3.14).

Input: $C_{j\alpha\beta}$

Output: $S_{ij}, C_{j\alpha\beta}$

```

1:  $S = 0$ 
2: for  $j = 1, \dots, r$  do
3:   for  $k = 1, \dots, j - 1$  do
4:      $S_{kj} = \sum_{\alpha,\beta} C_{k\alpha\beta} C_{j\alpha\beta}$ 
5:   for  $\alpha, \beta$  do
6:      $C_{j\alpha\beta} = C_{j\alpha\beta} - S_{kj} C_{k\alpha\beta}$ 
7:   end for
8: end for
9:  $S_{jj} = \sqrt{\sum_{\alpha,\beta} C_{j\alpha\beta}^2}$ 
10: for  $\alpha, \beta$  do
11:    $C_{j\alpha\beta} = C_{j\alpha\beta} / S_{jj}$ 
12: end for
13: end for
```

We have not yet discussed how to solve the evolution equations derived in this section. Equations (3.7) and (3.10) (which correspond to an advection in x_1 and x_2 , respectively) can be treated using the approach outlined in sections 2.1 and 2.2. That is, we can employ a spectral method or a semi-Lagrangian scheme. In fact, the present situation is simpler since the evolution equations only depend on a single variable. In fact, the further splitting into the different coordinate axis, as described in section 2.2 for the semi-Lagrangian approach, is not required in the present setting.

Before proceeding let us discuss the complexity of the proposed hierarchical low-rank splitting scheme. Solving the evolution equations (3.7) and (3.10) requires $\mathcal{O}(n\mathcal{R}^2)$ arithmetic operations and $\mathcal{O}(n\mathcal{R})$ storage, where n is the number of grid points (per direction) and $\mathcal{R} = \max(r, r_x, r_v, r_E)$. In addition, we have to compute the coefficients which requires $\mathcal{O}(n\mathcal{R}^2 + \mathcal{R}^4)$ arithmetic operations. The storage cost of the coefficients is $\mathcal{O}(n\mathcal{R}^2 + \mathcal{R}^4)$ and is dominated by a^3 and h^3 .

3.2. The hierarchical low-rank algorithm in six dimensions. In this section we extend the hierarchical low-rank approximation to the six-dimensional ($d = 3$) case. Since the derivation is very similar we will only state the relevant evolution equations here. We start with the low-rank representation

$$f(t, x, v) \approx \sum_{i,j} X_i(t, x) S_{ij}(t) V_j(t, v), \quad (3.15)$$

where $x = (x_1, x_2, x_3) \in \Omega_x \subset \mathbb{R}^3$, $v = (v_1, v_2, v_3) \in \Omega_v \subset \mathbb{R}^3$, and $S \in \mathbb{R}^{r \times r}$. We now restrict to the low-rank representation

$$X_i(t, x) = \sum_{\alpha, \beta, \gamma} C_{i\alpha\beta\gamma}(t) X_{1\alpha}(t, x_1) X_{2\beta}(t, x_2) X_{3\gamma}(t, x_3) \quad (3.16)$$

and

$$V_j(t, v) = \sum_{\alpha, \beta, \gamma} D_{j\alpha\beta\gamma}(t) V_{1\alpha}(t, v_1) V_{2\beta}(t, v_2) V_{3\gamma}(t, v_3), \quad (3.17)$$

where $C \in \mathbb{R}^{r \times r_x \times r_x \times r_x}$, $D \in \mathbb{R}^{r \times r_v \times r_v \times r_v}$ and r_x and r_v is the rank in the x - and v -direction, respectively. We then consider the evolution equation

$$\partial_t K_j(t, x) = - \sum_l c_{jl}^1 \cdot \nabla_x K_l(t, x) - \sum_l c_{jl}^2 \cdot F(K)(x) K_l(t, x),$$

which, depending on the choice of F , models either the update for X_i or V_j . Like in the previous section, we start with the initial value

$$K_j^0(x) = \sum_{\alpha, \beta, \gamma} C_{j\alpha\beta\gamma}^0 X_{1\alpha}^0(x_1) X_{2\beta}^0(x_2) X_{3\gamma}^0(x_3).$$

In the following we will divide the algorithm into four parts which correspond to the update of X_1 and C , the update of X_2 and C , the update of X_3 and C , and finally an update of C .

Step 1: We perform a QR decomposition

$$C_{j\alpha\beta\gamma}^0 = \sum_{\xi} Q_{j\xi\beta\gamma} R_{\alpha\xi}^0$$

and set

$$W_{j\alpha}(x_2, x_3) = \sum_{\beta, \gamma} Q_{j\alpha\beta\gamma} X_{2\beta}^0(x_2) X_{3\gamma}^0(x_3).$$

Then we define

$$M_{\alpha}(t, x_1) = \sum_{\xi} X_{1\xi}(t, x_1) R_{\xi\alpha}(t), \quad \text{with} \quad M_{\alpha}(0, x_1) = \sum_{\xi} X_{1\xi}^0(x_1) R_{\xi\alpha}^0,$$

for which we obtain the one-dimensional evolution equation

$$\partial_t M_{\alpha}(t, x_1) = - \sum_{\xi} a_{\alpha\xi}^1 \partial_{x_1} M_{\xi}(t, x_1) - \sum_{\xi} (a_{\alpha\xi}^2 + a_{\alpha\xi}^3(x_1)) M_{\xi}(t, x_1) \quad (3.18)$$

with

$$a_{\alpha\xi}^1 = \sum_{i,k} c_{ik}^{1;x_1} \langle W_{i\alpha}, W_{k\xi} \rangle_{x_2, x_3}, \quad a_{\alpha\xi}^2 = \sum_{i,k} \left(c_{ik}^{1;x_2} \langle W_{i\alpha}, \partial_{x_2} W_{k\xi} \rangle_{x_2, x_3} + c_{ik}^{1;x_3} \langle W_{i\alpha}, \partial_{x_3} W_{k\xi} \rangle_{x_2, x_3} \right)$$

and

$$a_{\alpha\xi}^3(x_1) = \sum_{i,k} c_{ik}^2 \cdot \langle W_{i\alpha}, F(M)(x_1, \cdot, \cdot) W_{k\xi} \rangle_{x_2, x_3}.$$

This is solved up to time τ . For the resulting functions $M_\alpha(\tau, x_1)$ a QR decomposition is performed to obtain orthonormal functions $X_{1\alpha}^1$ and the matrix $R_{\xi\alpha}^1$:

$$M_\alpha(\tau, x_1) = \sum_{\xi} X_{1\xi}^1(x_1) R_{\xi\alpha}^1.$$

Then we consider the matrix evolution equation for R ,

$$\dot{R}_{\xi\alpha}(t) = \sum_{\xi', \alpha'} b_{\xi\xi'}^1 R_{\xi'\alpha'}(t) a_{\alpha\alpha'}^1 + \sum_{\alpha'} R_{\xi\alpha'}(t) a_{\alpha\alpha'}^2 + \sum_{\xi', \alpha'} B_{\xi\alpha\xi'\alpha'} R_{\xi'\alpha'}(t) \quad (3.19)$$

with

$$b_{\xi\xi'}^1 = \langle X_{1\xi}^1, \partial_{x_1} X_{1\xi'}^1 \rangle_{x_1}, \quad B_{\xi\alpha\xi'\alpha'} = \sum_{i,k} c_{ik}^2 \cdot \langle X_{1\xi}^1 W_{i\alpha}, F(R) X_{1\xi'}^1 W_{k\alpha'} \rangle_x.$$

With a low-rank representation of $F(R)$, the three-dimensional integrals in the definition of $B_{\xi\alpha\xi'\alpha'}$ can again be broken up into linear combinations of products of one-dimensional integrals. Equation (3.19) with initial value R^1 is then integrated up to time τ to obtain $R^2 = R(\tau)$. Finally we obtain

$$C_{j\alpha\beta\gamma}^1 = \sum_{\xi} Q_{j\xi\beta\gamma} R_{\alpha\xi}^2.$$

Step 2: We perform a QR decomposition

$$C_{j\alpha\beta\gamma}^1 = \sum_{\eta} Q_{j\alpha\eta\gamma} R_{\beta\eta}^0,$$

where Q and R are different from those before, but nevertheless we use the same symbols for ease of notation. We set

$$W_{j\alpha\beta}(x_3) = \sum_{\gamma} Q_{j\alpha\beta\gamma} X_{3\gamma}^0(x_3).$$

Then we define

$$N_\beta(t, x_2) = \sum_{\eta} X_{2\eta}(t, x_2) R_{\eta\beta}(t)$$

for which we obtain the one-dimensional evolution equation

$$\partial_t N_\beta(t, x_2) = - \sum_{\eta} h_{\beta\eta}^1 \partial_{x_2} N_\eta(t, x_2) - \sum_{\eta} (h_{\beta\eta}^2 + h_{\beta\eta}^3(x_2)) N_\eta(t, x_2) \quad (3.20)$$

with

$$h_{\beta\eta}^1 = \sum_{i,k,\alpha} c_{ik}^{1;x_2} \langle W_{i\alpha\beta}, W_{k\alpha\eta} \rangle_{x_3}, \quad h_{\beta\eta}^2 = \sum_{i,k,\alpha,\xi} c_{ik}^{1;x_1} b_{\alpha\xi}^1 \langle W_{i\alpha\beta}, W_{k\xi\eta} \rangle_{x_3} + \sum_{i,k,\alpha} c_{ik}^{1;x_3} \langle W_{i\alpha\beta}, \partial_{x_3} W_{k\alpha\eta} \rangle_{x_3}$$

and

$$h_{\beta\eta}^3(x_2) = \sum_{i,k,\alpha,\xi} c_{ik}^2 \cdot \langle X_{1\alpha}^1 W_{i\alpha\beta}, F(N)(\cdot, x_2, \cdot) X_{1\xi}^1 W_{k\xi\eta} \rangle_{x_1, x_3}.$$

Equation (3.20) is then solved with initial value

$$N_\beta(0, x_2) = \sum_\eta X_{2\eta}^0(x_2) R_{\eta\beta}^0$$

up to time τ . For the resulting $N_\beta(\tau, x_2)$ a QR decomposition is performed to obtain $X_{2\eta}^1$ and $R_{\eta\beta}^1$.

Then we consider the matrix evolution equation for R ,

$$\dot{R}_{\eta\beta}(t) = \sum_{\eta', \beta'} b_{\eta\eta'}^2 R_{\eta'\beta'}(t) h_{\beta\beta'}^1 + \sum_{\beta'} R_{\eta\beta'}(t) h_{\beta\beta'}^2 + \sum_{\eta', \beta'} H_{\eta\beta\eta'\beta'} R_{\eta'\beta'}(t) \quad (3.21)$$

with

$$b_{\eta\eta'}^2 = \langle X_{2\eta}^1, \partial_{x_2} X_{2\eta'}^1 \rangle_{x_2}, \quad H_{\eta\beta\eta'\beta'} = \sum_{i,k,\xi,\xi'} c_{ik}^2 \cdot \langle X_{1\xi}^1 X_{2\eta}^1 W_{i\xi\beta}, F(R) X_{1\xi'}^1 X_{2\eta'}^1 W_{k\xi'\beta'} \rangle_x.$$

Equation (3.21) with initial value R^1 is integrated up to time τ to obtain R^2 . Finally, we obtain

$$C_{j\alpha\beta\gamma}^2 = \sum_\eta Q_{j\alpha\eta\gamma} R_{\beta\eta}^2.$$

Step 3: We perform a QR decomposition

$$C_{j\alpha\beta\gamma}^2 = \sum_\zeta Q_{j\alpha\beta\zeta} R_{\gamma\zeta}^0.$$

Then we define

$$O_\gamma(t, x_3) = \sum_\zeta X_{3\zeta}(t, x_3) R_{\zeta\gamma}(t)$$

for which we obtain the evolution equation

$$\partial_t O_\gamma(t, x_3) = - \sum_\zeta e_{\gamma\zeta}^1 \partial_{x_3} O_\zeta(t, x_3) - \sum_\zeta (e_{\gamma\zeta}^2 + e_{\gamma\zeta}^3(x_3)) O_\zeta(t, x_3) \quad (3.22)$$

with

$$e_{\gamma\zeta}^1 = \sum_{i,k,\alpha,\beta} c_{ik}^{1;x_3} Q_{i\alpha\beta\gamma} Q_{k\alpha\beta\zeta}, \quad e_{\gamma\zeta}^2 = \sum_{i,k,\alpha,\xi,\beta} c_{ik}^{1;x_1} b_{\alpha\xi}^1 Q_{i\alpha\beta\gamma} Q_{k\xi\beta\zeta} + \sum_{i,k,\alpha,\beta,\eta} c_{ik}^{1;x_2} b_{\beta\eta}^2 Q_{i\alpha\beta\gamma} Q_{k\alpha\eta\zeta}$$

and

$$e_{\gamma\zeta}^3(x_3) = \sum_{i,k,\alpha,\xi,\beta,\eta} c_{ik}^2 \cdot \langle X_{1\alpha} X_{2\beta}, F(O)(\cdot, \cdot, x_3) X_{1\xi} X_{2\eta} \rangle_{x_1, x_2} Q_{i\alpha\beta\gamma} Q_{k\xi\eta\zeta}.$$

Equation (3.22) is then solved with initial value

$$O_\gamma(0, x_3) = \sum_\zeta X_{3\zeta}^0(x_3) R_{\zeta\gamma}^0$$

up to time τ . For the resulting $O_\gamma(\tau, x_2)$ a QR decomposition is performed to obtain $X_{3\zeta}^1$ and $R_{\zeta\gamma}^1$.

Then we consider the evolution equation for R ,

$$\dot{R}_{\zeta\gamma}(t) = \sum_{\zeta', \gamma'} b_{\zeta\zeta'}^3 R_{\zeta'\gamma'}(t) e_{\gamma\gamma'}^1 + \sum_{\gamma'} R_{\zeta\gamma'}(t) e_{\gamma\gamma'}^2 + \sum_{\zeta', \gamma'} G_{\zeta\gamma\zeta'\gamma'} R_{\zeta'\gamma'}(t) \quad (3.23)$$

with

$$b_{\gamma\zeta'}^3 = (X_{3\gamma}, \partial_{x_3} X_{3\zeta'}), \quad G_{\zeta\gamma\zeta'\gamma'} = \sum_{i,k,\alpha,\beta,\alpha',\beta'} c_{ik}^2 \cdot \langle X_{1\alpha}^1 X_{2\beta}^1 X_{3\zeta}^1, F(R) X_{1\alpha'}^1 X_{2\beta'}^1 X_{3\zeta'}^1 \rangle_x Q_{i\alpha\beta\gamma} Q_{k\alpha'\beta'\gamma'}.$$

Equation (3.23) with initial value R^1 is integrated up to time τ to obtain R^2 . Finally we obtain

$$C_{j\alpha\beta\gamma}^3 = \sum_{\gamma} Q_{j\alpha\beta\zeta} R_{\gamma\zeta}^2.$$

Step 4: The final step directly updates C . The corresponding evolution equation is

$$\dot{C}_{i\alpha\beta\gamma}(t) = \sum_{k,\xi} c_{ik}^{1;x_1} b_{\alpha\xi}^1 C_{k\xi\beta\gamma}(t) + \sum_{k,\eta} c_{ik}^{1;x_2} b_{\beta\eta}^2 C_{k\alpha\eta\gamma}(t) + \sum_{k,\zeta} c_{ik}^{1;x_3} b_{\gamma\zeta}^3 C_{k\alpha\beta\zeta}(t) + \sum_{k,\xi,\eta,\zeta} (c_{ik}^2 \cdot e_{\alpha\beta\gamma\xi\eta\zeta}) C_{k\xi\eta\zeta}(t) \quad (3.24)$$

with

$$e_{\alpha\beta\gamma\xi\eta\zeta} = \langle X_{1\alpha}^1 X_{2\beta}^1 X_{3\gamma}^1, F(R) X_{1\xi}^1 X_{2\eta}^1 X_{3\zeta}^1 \rangle_x.$$

Equation (3.24) with initial value C^3 is then solved up to time τ to obtain C^4 . This completes a full time step of algorithm. The output is

$$K_j(\tau, x) \approx K_j^1(x) = \sum_{\alpha,\beta,\gamma} C_{j\alpha\beta\gamma}^4 X_{1\alpha}^1(x_1) X_{2\beta}^1(x_2) X_{3\gamma}^1(x_3).$$

At the end, a factorization into an orthogonalized tensor C and a matrix S is obtained as in Algorithm 2, simply by adding a subscript γ to every appearance of α, β in that algorithm.

4. Numerical results. In this section we show numerical results for the low-rank and the hierarchical low-rank splitting algorithm. In both cases the spectral method described in section 2.1 is used. Numerical results for linear Landau damping, for a two-stream instability and a plasma echo will be presented.

4.1. Linear Landau damping. First, let us consider the classic two-dimensional Landau damping. We set $\Omega = \Omega_x \times \Omega_v = (0, 4\pi) \times (-6, 6)$ and impose the initial value

$$f_0(x, v) = \frac{1}{\sqrt{2\pi}} e^{-v^2/2} (1 + \alpha \cos(kx)),$$

where we have chosen $\alpha = 10^{-2}$ and $k = \frac{1}{2}$. In both the x - and v -direction periodic boundary conditions are imposed. It can be shown by a linear analysis that the decay rate of the electric energy is given by $\gamma \approx -0.153$. The so obtained decay rate has been verified by a host of numerical simulations presented in the literature. The numerical results obtained using the low-rank/FFT algorithm proposed in Section 2.1 are shown in Figure 4.1.

We observe that choosing the rank $r = 5$ is sufficient to obtain a numerical solution which very closely matches the analytic result. Although we see that the numerical method does not conserve energy up to machine precision, the error is very small (on the order of 10^{-8}). In addition, the errors in mass and in the L^2 norm are indistinguishable from machine precision.

Next, we turn our attention to a four-dimensional problem. That is, we set $\Omega = (0, 4\pi)^2 \times (-6, 6)^2$ and impose the initial value

$$f_0(x, y, v, w) = \frac{1}{2\pi} e^{-(v^2+w^2)/2} (1 + \alpha \cos(k_1 x) + \alpha \cos(k_2 y)),$$

where we have chosen $\alpha = 10^{-2}$ and $k_1 = k_2 = \frac{1}{2}$. As before, periodic boundary conditions are chosen for all directions. Although the problem is now set in four dimensions, the behavior of the electric energy is almost identical to the two-dimensional problem. The numerical results obtained using the hierarchical

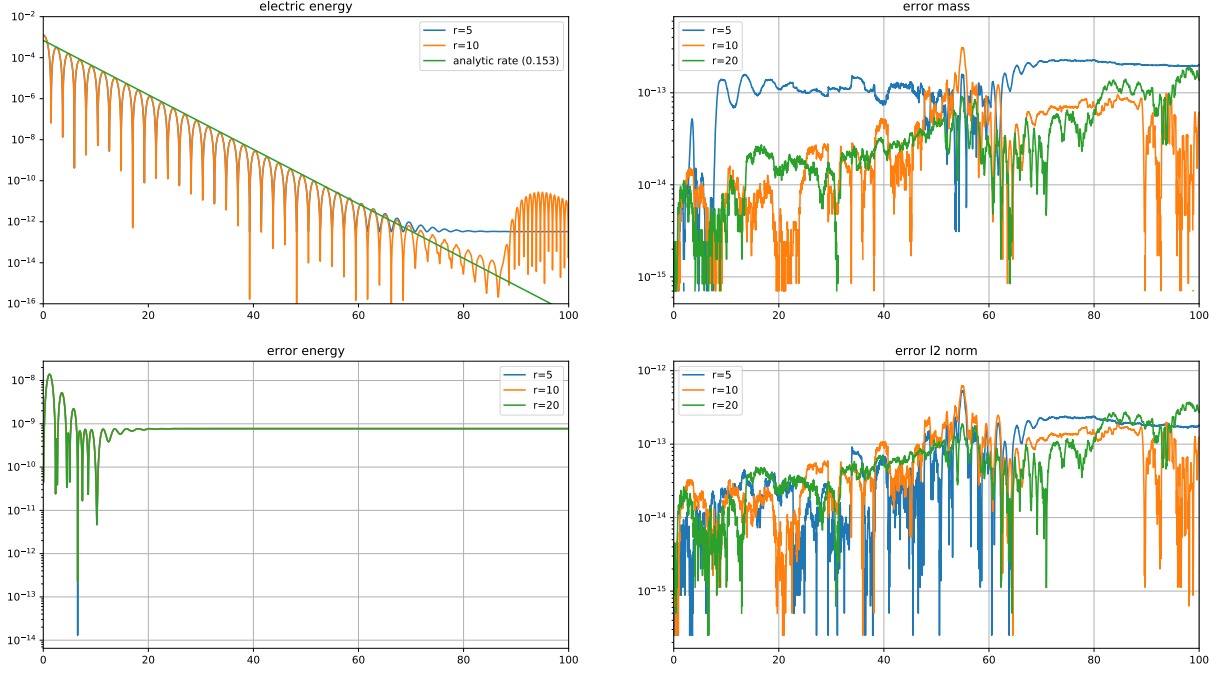


FIGURE 4.1. Numerical simulations of linear Landau damping with the low-rank/FFT algorithm and various ranks are shown (note that the plots for $r = 10$ and $r = 20$ in the top left figure are indistinguishable). The Strang splitting algorithm with a time step size $\tau = 0.025$ is employed. In the x -direction 64 grid points are used, while in the v -direction 256 grid points are used.

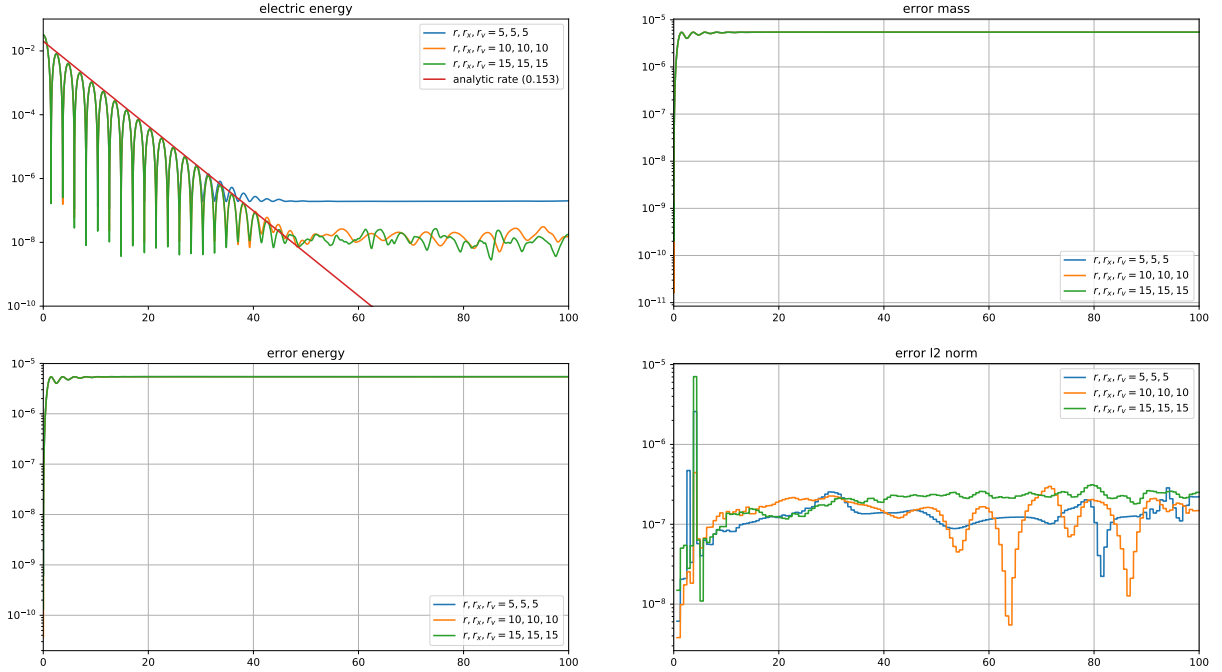


FIGURE 4.2. Numerical simulations of four-dimensional linear Landau damping with the hierarchical low-rank/FFT algorithm and various ranks are shown (note that the error in mass and energy is almost identical for all three configurations). The Lie-Trotter splitting algorithm with a time step size $\tau = 0.00625$ is employed. In the x -direction 64 grid points are used, while in the v -direction 256 grid points are used. The L^2 norm is only computed for every 40th time step.

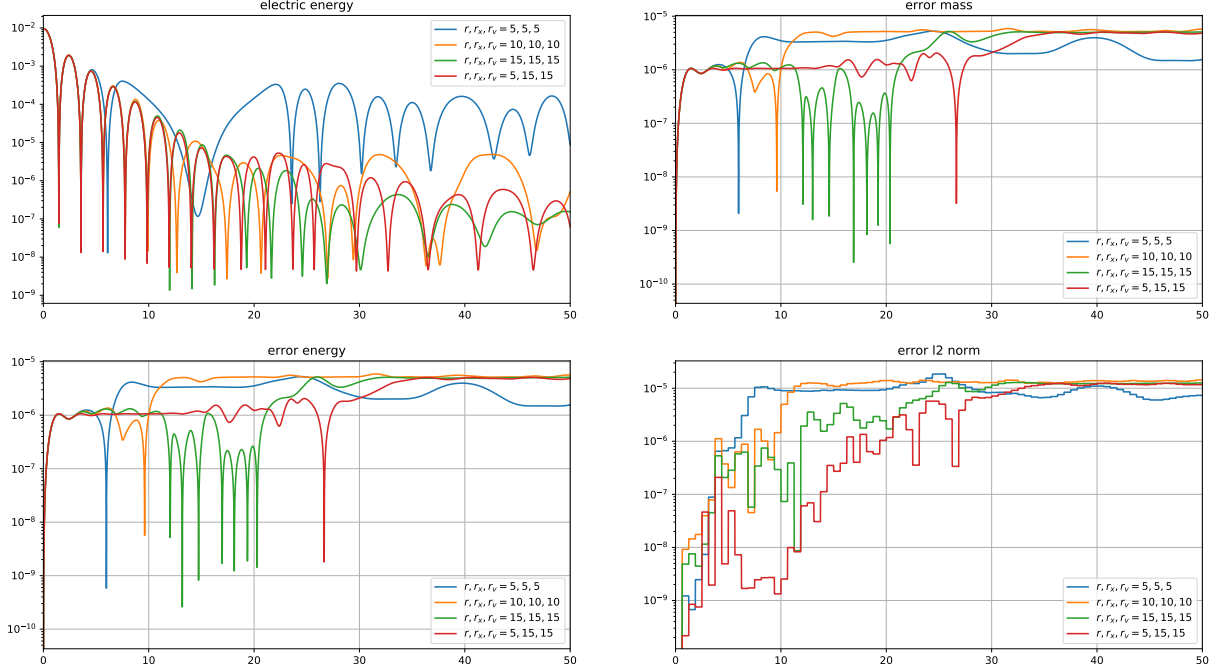


FIGURE 4.3. Numerical simulations of the four-dimensional non-aligned linear Landau damping with the hierarchical low-rank/FFT algorithm and various ranks are shown (note that the error in mass and energy is almost identical for all three configurations). The Lie–Trotter splitting algorithm with a time step size $\tau = 0.00625$ is employed. In the x -direction 64 grid points are used, while in the v -direction 256 grid points are used. The L^2 norm is only computed for every 100th time step.

low-rank algorithm proposed in section 3 are shown in Figure 4.2. We observe that the simulation with rank $(r, r_x, r_v) = (5, 5, 5)$ is already able to correctly predict the decay rate. Considering the simulation with $(r, r_x, r_v) = 10$ shows a reduction in the electric energy to 10^{-8} which is approximately two orders of magnitude better compared to the configuration with rank $(r, r_x, r_v) = (5, 5, 5)$. In all configurations mass, energy, and the L^2 norm are conserved up to an error less than 10^{-6} .

To conclude the discussion on Landau damping, we consider a setting in which the perturbation is not aligned to the coordinate axis. More specifically, we consider $\Omega = (0, 5\pi)^2 \times (-6, 6)^2$ and impose the initial value

$$f_0(x, y, v, w) = \frac{1}{2\pi} e^{-(v^2 + w^2)/2} (1 + \alpha \cos(k_1 x) \cos(k_2 y)),$$

where we have chosen $\alpha = 10^{-2}$ and $k_1 = k_2 = 0.4$. As before, periodic boundary conditions are chosen for all directions. The numerical results obtained using the hierarchical low-rank algorithm proposed in section 3 are shown in Figure 4.3. We observe that the simulation with rank $(r, r_x, r_v) = (10, 10, 10)$ and $(r, r_x, r_v) = (15, 15, 15)$ show a reduction of the electric energy to $5 \cdot 10^{-6}$ and $5 \cdot 10^{-7}$, respectively. We also note that r can be chosen significantly smaller than r_x and r_v , while still obtaining good results. For all configurations the error in mass, energy, and L^2 norm is below 10^{-5} .

4.2. Two-stream instability. Our second numerical example is the so-called two-stream instability. Here we have two beams propagating in opposite directions. This setup is an unstable equilibrium and small perturbations in the initial particle-density function eventually force the electric energy to increase exponentially. This is called the linear regime. At some later time saturation sets in (the nonlinear regime). This phase is characterized by nearly constant electric energy and significant filamentation of the phase space.

First we consider the two-dimensional case. We thus set $\Omega = (0, 10\pi) \times (-9, 9)$ and impose the initial

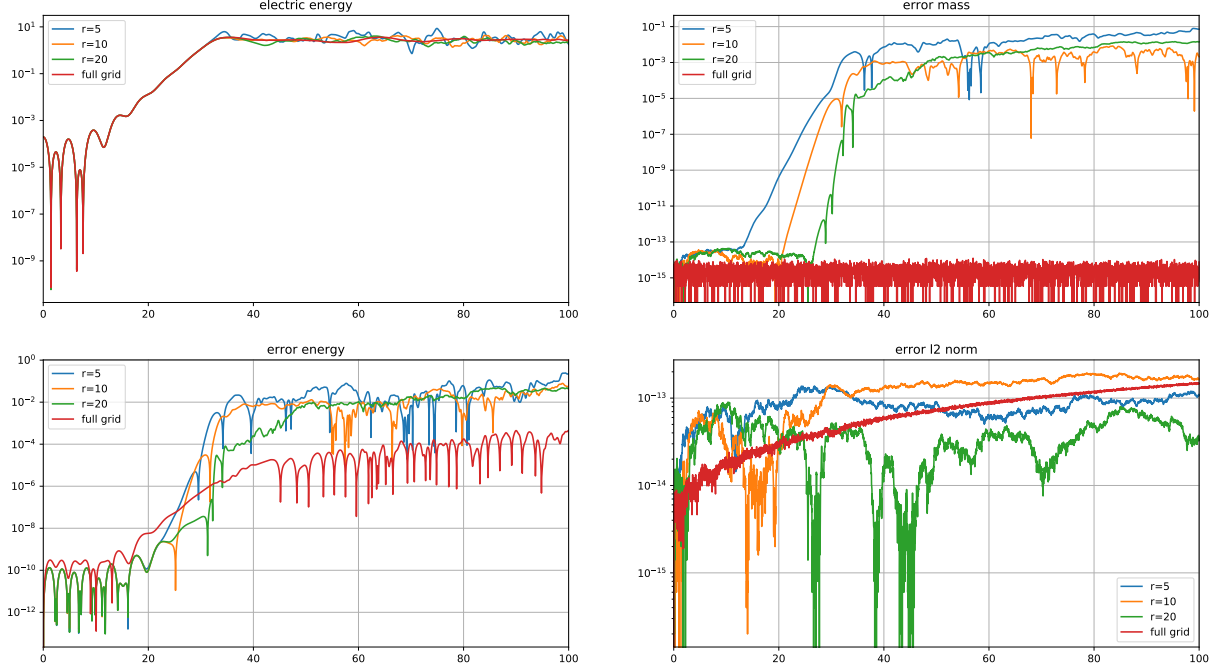


FIGURE 4.4. Numerical simulations of the two-dimensional two-stream instability with the low-rank/FFT algorithm and various ranks are shown. The Strang splitting algorithm with a time step size $\tau = 0.025$ is employed. In both the x and v -directions 128 grid points are used. As comparison a direct Eulerian simulation with a splitting/discontinuous Galerkin semi-Lagrangian scheme is also shown.

condition

$$f_0(x, v) = \frac{1}{2\sqrt{2\pi}} \left(e^{-(v-v_0)^2/2} + e^{-(v+v_0)^2/2} \right) (1 + \alpha \cos(kx)),$$

where $\alpha = 10^{-3}$, $k = \frac{1}{5}$, and $v_0 = 2.4$. As before, periodic boundary conditions are used. The corresponding numerical simulations obtained using the low-rank/FFT algorithm proposed in Section 2.1 are shown in Figure 4.4. In the linear regime excellent agreement between the direct Eulerian simulation and the solution with rank $r = 5$ is observed. As we enter the nonlinear regime all the solutions become somewhat distinct. However, due to the chaotic nature of this regime this is not surprising. The figure of merit we are looking at in the nonlinear regime is if the numerical scheme is able to keep the electric energy approximately constant. All configurations starting from rank $r = 10$ do this very well.

To further evaluate the quality of the numerical solution, let us consider the physical invariants. By looking at Figure 4.4, it becomes clear that from this standpoint the two-stream instability is a significantly more challenging problem than the linear Landau damping considered in the previous section. However, it should be noted that most of the error in mass and energy is accrued during the exponential growth of the electric energy but remains essentially unchanged in the nonlinear phase. In particular, there is no observable long-term drift in the error of any of the invariants. With respect to energy, the low-rank approximation with $r = 10$ is worse by approximately two orders of magnitude compared to the direct Eulerian simulation (which has been conducted using a FFT based implementation). The L^2 norm is conserved up to machine precision.

Second, we turn our attention to the four-dimensional case. We set $\Omega = (0, 10\pi)^2 \times (-9, 9)^2$ and impose the initial condition

$$f_0(x, y, v, w) = \frac{1}{8\pi} \left(e^{-(v-v_0)^2/2} + e^{-(v+v_0)^2/2} \right) \left(e^{-(w-w_0)^2/2} + e^{-(w+w_0)^2/2} \right) (1 + \alpha_1 \cos(k_1 x) + \alpha_2 \cos(k_2 y))$$

with $\alpha_1 = \alpha_2 = 10^{-3}$, $k_1 = k_2 = \frac{1}{5}$, $v_0 = w_0 = 2.4$. As before, periodic boundary conditions are employed in all directions. We note that this configuration corresponds to four propagating beams. The numerical

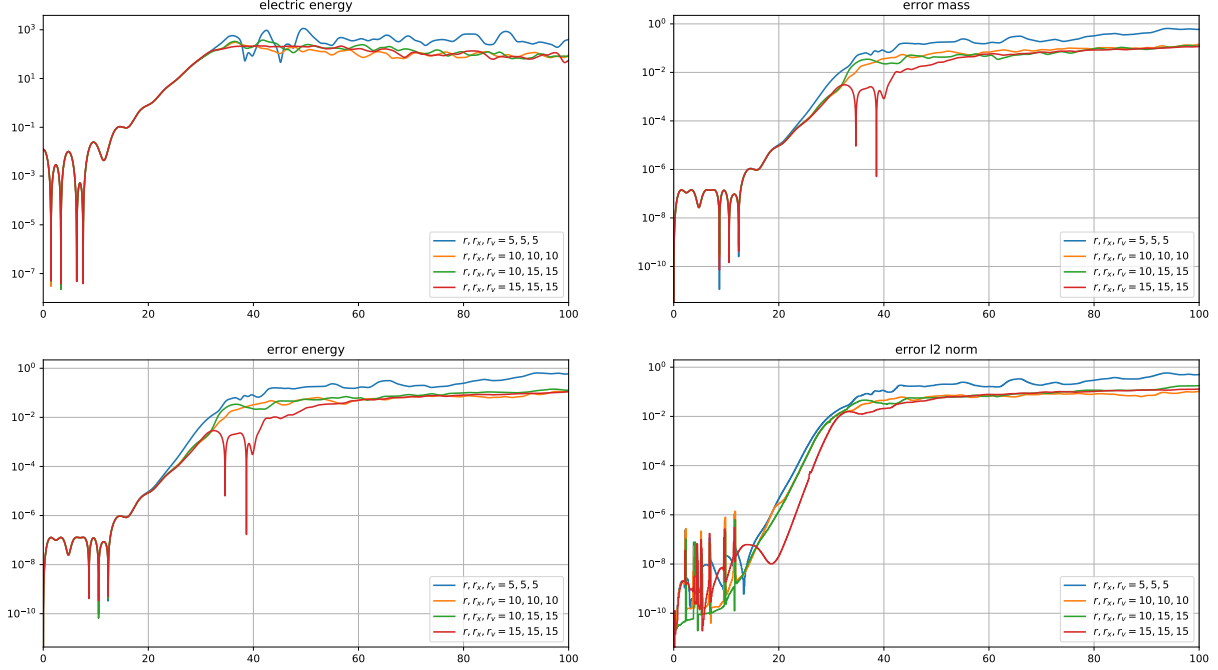


FIGURE 4.5. Numerical simulations of the four-dimensional two-stream instability with the hierarchical low-rank/FFT algorithm and various ranks are shown. The Lie-Trotter projector-splitting algorithm with a time step size $\tau = 0.00625$ is employed. In both the x - and v -directions 128 grid points are used. The L^2 norm is only computed for every 100th time step.

results obtained using the hierarchical low-rank algorithm proposed in section 3 are shown in Figure 4.5. The obtained results are similar to the two-dimensional case. In particular, in the linear regime we observe excellent agreement even for $(r, r_x, r_v) = (5, 5, 5)$. The errors in mass, energy, and L^2 norm are approximately one order of magnitude better for the configuration with $(r, r_x, r_v) = (10, 10, 10)$ compared to $(r, r_x, r_v) = (5, 5, 5)$.

4.3. Plasma echo. There are problems that need to resolve Landau damping for relatively long times. It is well known that due to the recurrence effect the number of grid points n_v in each coordinate direction of v has to scale as $n_v \propto T$, where T is the final time of the simulation (although this can be somewhat alleviated by using filamentation filtration techniques; see, for example, [30, 15]). Due to the high number of grid points required to conduct such simulation the proposed algorithm can be extremely efficient in this context. We will now consider such an example, the plasma echo phenomenon (see, for example, [21, 27, 15]).

We consider the domain $(0, 100) \times (-8, 8)$ and impose the initial condition

$$f_0(x, v) = \frac{1}{2\pi} e^{-v^2/2} (1 + \alpha \cos(k_1 x)),$$

where $\alpha = 10^{-3}$ and $k_1 = 12\pi/100$. As before, periodic boundary conditions are used. The initial perturbation in the electric field is damped away by Landau damping. Then at time $t_2 = 200$ we add another perturbation of the form

$$\frac{\alpha}{2\pi} e^{-v^2/2} \cos(k_2 x),$$

where $k_2 = 24\pi/100$. The corresponding perturbation in the electric field is, again, damped away. However, the particle-density function retains all the information regarding the two perturbations. As a consequence, at later times an echo (a peak in the amplitude of the electric field) occurs. The time of the echo depends on the wave numbers of the two perturbations. In the present case we expect a primary echo at $t = 400$ and a secondary echo at $t = 800$. This setup has been considered in [27] and [15].

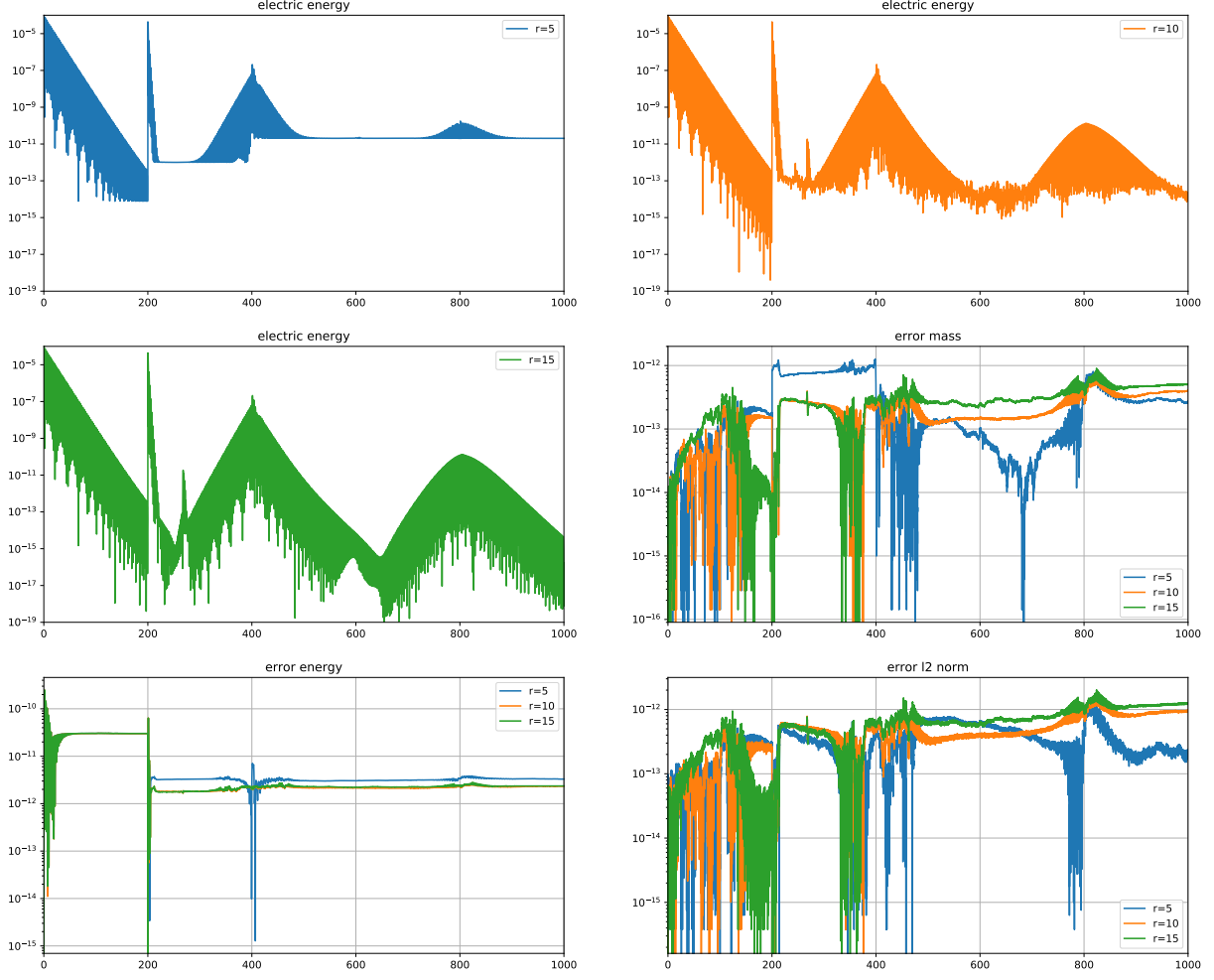


FIGURE 4.6. Numerical simulations of the two-dimensional plasma echo with the low-rank/FFT algorithm and various ranks are shown. The Strang projector-splitting algorithm with a time step size $\tau = 0.025$ is employed. In the x - and v -direction 512 and 4096 grid points are used, respectively. Note that due to the second perturbation, we restart the computation of the errors in mass, energy, and L^2 norm at $t = 200$.

The corresponding numerical simulations are shown in Figure 4.6. Even for $r = 5$ both the primary and the secondary echo are clearly resolved. This holds true even though the electric energy is only resolved up to an amplitude of approximately 10^{-11} and the magnitude of the secondary echo is only slightly above that threshold. Increasing the rank (to $r = 10$) then allows us to resolve the growth and decay of the electric energy associated with the secondary echo as well. Since this problem requires only a small rank but a large number of grid points (4096 grid points are used in the velocity direction and 512 grid points are used in the space direction), the computational effort required is reduced by a significant margin. Let us also note that, for all configurations considered here, the conservation of mass, energy, and L^2 norm is excellent (below 10^{-10}).

Overall, the results presented here for Landau damping, the two-stream instability, and the plasma echo, show that significant reduction in computational effort can be obtained compared with performing a direct simulation. In fact, all simulations have been performed on a somewhat outdated workstation and no effort has been made to parallelize the code.

REFERENCES

- [1] A. Arnold and T. Jahnke. On the approximation of high-dimensional differential equations in the hierarchical Tucker format. *BIT Numerical Mathematics*, 54(2):305–341, 2014.
- [2] J. Bigot, V. Grandgirard, G. Latu, C. Passeron, F. Rozar, and O. Thomine. Scaling GYSELA code beyond 32K-cores on Blue Gene/Q. In *ESAIM: Proceedings*, volume 43, pages 117–135, 2013.
- [3] C. Cheng and G. Knorr. The integration of the Vlasov equation in configuration space. *J. Comput. Phys.*, 22(3):330–351, 1976.
- [4] D. Conte and C. Lubich. An error analysis of the multi-configuration time-dependent Hartree method of quantum dynamics. *ESAIM Math. Model. Numer. Anal.*, 44(4):759–780, 2010.
- [5] N. Crouseilles, L. Einkemmer, and E. Faou. Hamiltonian splitting for the Vlasov–Maxwell equations. *J. Comput. Phys.*, 283:224–240, 2015.
- [6] N. Crouseilles, L. Einkemmer, and E. Faou. An asymptotic preserving scheme for the relativistic Vlasov–Maxwell equations in the classical limit. *Comput. Phys. Commun.*, 209:13–26, 2016.
- [7] N. Crouseilles, L. Einkemmer, and M. Prugger. An exponential integrator for the drift-kinetic model. *arXiv:1705.09923*, 2017.
- [8] N. Crouseilles, G. Latu, and E. Sonnendrücker. A parallel Vlasov solver based on local cubic spline interpolation on patches. *J. Comput. Phys.*, 228(5):1429–1446, 2009.
- [9] N. Crouseilles, M. Mehrenberger, and F. Vecil. Discontinuous Galerkin semi-Lagrangian method for Vlasov-Poisson. In *ESAIM: Proceedings*, volume 32, pages 211–230, 2011.
- [10] E. Deriaz and S. Peirani. Six-dimensional adaptive simulation of the Vlasov equations using a hierarchical basis. *hal-01419750*, 2016.
- [11] L. Einkemmer. A mixed precision semi-Lagrangian algorithm and its performance on accelerators. In *High Performance Computing & Simulation (HPCS), 2016 International Conference on*, pages 74–80, 2016.
- [12] L. Einkemmer. High performance computing aspects of a dimension independent semi-Lagrangian discontinuous Galerkin code. *Comput. Phys. Commun.*, 202:326–336, 2016.
- [13] L. Einkemmer. A study on conserving invariants of the Vlasov equation in semi-Lagrangian computer simulations. *J. Plasma Phys.*, 83(2), 2017.
- [14] L. Einkemmer. A comparison of semi-Lagrangian discontinuous Galerkin and spline based Vlasov solvers in four dimensions. *arXiv preprint, arXiv:1803.02143*, 2018.
- [15] L. Einkemmer and A. Ostermann. A strategy to suppress recurrence in grid-based Vlasov solvers. *Eur. Phys. J. D*, 68(7):197, 2014.
- [16] L. Einkemmer and A. Ostermann. An almost symmetric Strang splitting scheme for nonlinear evolution equations. *Comput. Math. Appl.*, 67(12):2144–2157, 2014.
- [17] L. Einkemmer and A. Ostermann. An almost symmetric Strang splitting scheme for the construction of high order composition methods. *Comput. Appl. Math.*, 271:307–318, 2014.
- [18] E. Fijalkow. A numerical solution to the Vlasov equation. *Comput. Phys. Commun.*, 116(2-3):319–328, 1999.
- [19] F. Filbet and E. Sonnendrücker. Comparison of Eulerian Vlasov solvers. *Comput. Phys. Commun.*, 150(3):247–266, 2003.
- [20] F. Filbet, E. Sonnendrücker, and P. Bertrand. Conservative numerical schemes for the Vlasov equation. *J. Comput. Phys.*, 172(1):166–187, 2001.
- [21] R.W. Gould, T.M. O’Neil, and J.H. Malmberg. Plasma wave echo. *Phys. Rev. Lett.*, 19(5):219–222, 1967.
- [22] V. Grandgirard, J. Abiteboul, J. Bigot, T. Cartier-Michaud, N. Crouseilles, G. Dif-Pradalier, Ch. Ehrlacher, D. Esteve, X. Garbet, Ph. Ghendrih, G. Latu, M. Mehrenberger, C. Norscini, C. Passeron, F. Rozar, Y. Sarazin, E. Sonnendrücker, A. Strugarek, and D. Zarzoso. A 5D gyrokinetic full-f global semi-Lagrangian code for flux-driven ion turbulence simulations. *Comput. Phys. Commun.*, 207:35–68, 2016.
- [23] V. Grandgirard, M. Brunetti, P. Bertrand, N. Besse, X. Garbet, P. Ghendrih, G. Manfredi, Y. Sarazin, O. Sauter, E. Sonnendrücker, J. Vaclavik, and L. Villard. A drift-kinetic Semi-Lagrangian 4D code for ion turbulence simulation. *J. Comput. Phys.*, 217(2):395–423, 2006.
- [24] We. Guo and Y. Cheng. A sparse grid discontinuous Galerkin method for high-dimensional transport equations and its application to kinetic simulation. *SIAM J. Sci. Comput.*, 38(6):3381–3409, 2016.
- [25] J. Haegeman, C. Lubich, I. Oseledets, B. Vandereycken, and F. Verstraete. Unifying time evolution and optimization with matrix product states. *Physical Review B*, 94(16):165116, 2016.
- [26] M. Hochbruck and A. Ostermann. Exponential integrators. *Acta Numer.*, 19:209–286, 2010.
- [27] Y.W. Hou, Z.W. Ma, and M.Y. Yu. The plasma wave echo revisited. *Phys. Plasmas*, 18(1):012108, 2011.
- [28] T. Jahnke and W. Huisinga. A dynamical low-rank approach to the chemical master equation. *Bulletin of mathematical biology*, 70(8):2283–2302, 2008.
- [29] E. Kieri, C. Lubich, and H. Walach. Discretized dynamical low-rank approximation in the presence of small singular values. *SIAM J. Numer. Anal.*, 54(2):1020–1038, 2016.
- [30] A.J. Klimas and W.M. Farrell. A splitting algorithm for Vlasov simulation with filamentation filtration. *J. Comput. Phys.*, 110(1):150–163, 1994.
- [31] O. Koch and C. Lubich. Dynamical low-rank approximation. *SIAM J. Matrix Anal. Appl.*, 29(2):434–454, 2007.
- [32] O. Koch and C. Lubich. Dynamical tensor approximation. *SIAM J. Matrix Anal. Appl.*, 31(5):2360–2375, 2010.
- [33] K. Kormann. A semi-Lagrangian Vlasov solver in tensor train format. *SIAM J. Sci. Comput.*, 37(4):613–632, 2015.
- [34] K. Kormann and E. Sonnendrücker. Sparse grids for the Vlasov–Poisson equation. *Sparse Grids Appl.*, pages 163–190, 2014.
- [35] G. Latu, N. Crouseilles, V. Grandgirard, and E. Sonnendrücker. Gyrokinetic semi-lagrangian parallel simulation using a

- hybrid OpenMP/MPI programming. In *14th European PVM/MPI Users' Group Meeting*, pages 356–364, 2007.
- [36] C. Lubich. *From quantum to classical molecular dynamics: reduced models and numerical analysis*. European Mathematical Society, 2008.
 - [37] C. Lubich. Time integration in the multiconfiguration time-dependent Hartree method of molecular quantum dynamics. *Applied Mathematics Research eXpress*, 2015(2):311–328, 2015.
 - [38] C. Lubich, I. V. Oseledets, and B. Vandereycken. Time integration of tensor trains. *SIAM J. Numer. Anal.*, 53(2):917–941, 2015.
 - [39] C. Lubich and I.V. Oseledets. A projector-splitting integrator for dynamical low-rank approximation. *BIT Numer. Math.*, 54(1):171–188, 2014.
 - [40] C. Lubich, T. Rohwedder, R. Schneider, and B. Vandereycken. Dynamical approximation by hierarchical Tucker and tensor-train tensors. *SIAM J. Matrix Anal. Appl.*, 34(2):470–494, 2013.
 - [41] C. Lubich, B. Vandereycken, and H. Walach. Time integration of rank-constrained Tucker tensors. *Preprint, arXiv:1709.02594*, 2017.
 - [42] M. Mehrenberger, C. Steiner, L. Marradi, N. Crouseilles, E. Sonnendrucker, and B. Afeyan. Vlasov on GPU (VOG project). *arXiv:1301.5892*, 2013.
 - [43] H. Mena, A. Ostermann, L. Pfurtscheller, and C. Piazzola. Numerical low-rank approximation of matrix differential equations. *arXiv:1705.10175*, 2017.
 - [44] H.-D. Meyer, F. Gatti, and G. A. Worth. *Multidimensional quantum dynamics*. John Wiley & Sons, 2009.
 - [45] H.-D. Meyer, U. Manthe, and L. S. Cederbaum. The multi-configurational time-dependent Hartree approach. *Chem. Phys. Letters*, 165(1):73–78, 1990.
 - [46] P. J. Morrison. Structure and structure-preserving algorithms for plasma physics. *Cit. Phys. Plasmas*, 24(055502), 2017.
 - [47] E. Musharbash and F. Nobile. Dual dynamically orthogonal approximation of incompressible navier stokes equations with random boundary conditions. *J. Comp. Phys.*, 354:135–162, 2018.
 - [48] A. Nonnenmacher and C. Lubich. Dynamical low-rank approximation: applications and numerical experiments. *Mathematics and Computers in Simulation*, 79(4):1346–1357, 2008.
 - [49] J.M. Qiu and C.W. Shu. Positivity preserving semi-Lagrangian discontinuous Galerkin formulation: theoretical analysis and application to the Vlasov–Poisson system. *J. Comput. Phys.*, 230(23):8386–8409, 2011.
 - [50] J.A. Rossmannith and D.C. Seal. A positivity-preserving high-order semi-Lagrangian discontinuous Galerkin scheme for the Vlasov–Poisson equations. *J. Comput. Phys.*, 230(16):6203–6232, 2011.
 - [51] F. Rozar, G. Latu, and J. Roman. Achieving memory scalability in the GYSELA code to fit exascale constraints. In *Parallel Processing and Applied Mathematics*, pages 185–195. 2013.
 - [52] N. J. Sircombe and T. D. Arber. VALIS: A split-conservative scheme for the relativistic 2D Vlasov–Maxwell system. *J. Comput. Phys.*, 228(13):4773–4788, 2009.
 - [53] E. Sonnendrücker, J. Roche, P. Bertrand, and A. Ghizzo. The semi-Lagrangian method for the numerical resolution of the Vlasov equation. *J. Comput. Phys.*, 149(2):201–220, 1999.
 - [54] J. P. Verboncoeur. Particle simulation of plasmas: review and advances. *Plasma Physics and Controlled Fusion*, 47(5A):A231, 2005.